

$K \rightarrow 3\pi$ Final State Interactions at NLO in CHPT and Cabibbo's Proposal to Measure $a_0 - a_2$

Elvira Gámiz

*Department of Physics and Astronomy, The University of Glasgow, Glasgow G12 8QQ,
United Kingdom*

Joaquim Prades

*CAFPE and Departamento de Física Teórica y del Cosmos, Universidad de Granada,
Campus de Fuente Nueva, E-18002 Granada, Spain*

Ignazio Scimemi

*Departament de Física Teòrica, IFIC, CSIC-Universitat de València,
Apt. de Correus 22085, E-46071 València, Spain*

ABSTRACT: We present the analytical results for the $K \rightarrow 3\pi$ final state interactions at next-to-leading order (NLO) in CHPT. We also study the recent Cabibbo's proposal to measure the $\pi\pi$ scattering lengths combination $a_0 - a_2$ from the cusp effect in the $\pi^0\pi^0$ energy spectrum at threshold for $K^+ \rightarrow \pi^+\pi^0\pi^0$ and $K_L \rightarrow \pi^0\pi^0\pi^0$, and give the relevant formulas to describe it at NLO. For that, we use the NLO CHPT expression to fit the real part of $K \rightarrow 3\pi$ to data while the $\pi\pi$ scattering lengths are treated non-perturbatively. Using them, we make a quantitative estimate of the theoretical uncertainty of the $a_0 - a_2$ determination at NLO in our approach and obtain that it is not smaller than 5 % if added quadratically and 7 % if linearly for $K^+ \rightarrow \pi^+\pi^0\pi^0$. One gets similar theoretical uncertainties if the neutral $K_L \rightarrow \pi^0\pi^0\pi^0$ decays data below threshold are used instead. For this decay, there are very large theoretical uncertainties above threshold due to cancellations and these data cannot be used to get the scattering lengths. All the numbers we present are in the isospin limit. We compare our results for the cusp effect with Cabibbo and Isidori's results and discuss the differences.

KEYWORDS: Kaon Physics, Chiral Lagrangians, QCD.

Contents

1. Introduction	1
2. Notation	3
3. FSI for $K \rightarrow 3 \pi$ at NLO	5
4. Cabibbo's Proposal at NLO in CHPT	6
4.1 Cabibbo's Proposal for Charged Kaon Decays	9
4.2 Cabibbo's Proposal for Neutral Kaons	15
5. Summary and Conclusions	18
A. Numerical Inputs	20
B. FSI at NLO for Neutral Kaon Decays: Two-Pion Cuts	21
B.1 Notation	21
B.2 FSI for $K_L \rightarrow \pi^0 \pi^0 \pi^0$ at NLO	22
B.3 FSI for $K_L \rightarrow \pi^+ \pi^- \pi^0$ at NLO	23
B.4 FSI for $K_S \rightarrow \pi^+ \pi^- \pi^0$ at NLO	24
C. Three-Pion Cut Contributions to FSI	25

1. Introduction

Final state interactions (FSI) at next-to-leading order (NLO) in Chiral Perturbation Theory¹ (CHPT) [3, 4] are needed to obtain the charged CP-violating asymmetries at NLO [5, 6, 7]. The dominant contribution to these $K^+ \rightarrow 3\pi$ FSI at NLO are from two-pion cuts for topology A in Figure 1. They were calculated analytically in [5].

Though to get the full $K \rightarrow 3\pi$ amplitudes at order p^6 implies a two-loop calculation, one can get the FSI at NLO using the optical theorem within CHPT with the advantage that one just needs to know $\pi\pi$ scattering and $K \rightarrow 3\pi$ both at $\mathcal{O}(p^4)$. Notice that NLO in the dispersive part of the amplitude means one-loop and $\mathcal{O}(p^4)$ in CHPT while NLO in the absorptive part of the amplitude means two-loops and $\mathcal{O}(p^6)$ in CHPT.

In [5], we took the $\pi\pi$ scattering results from [8] and calculated the amplitudes $K \rightarrow 3\pi$ at NLO in the isospin limit. We agreed with the NLO $K \rightarrow 3\pi$ results recently published in [9]. These were previously calculated in [10] and used in [11], but unfortunately the analytical full results were not available there. Now, there is also available the full one-loop

¹Some introductory lectures on CHPT can be found in [1] and recent reviews in [2].

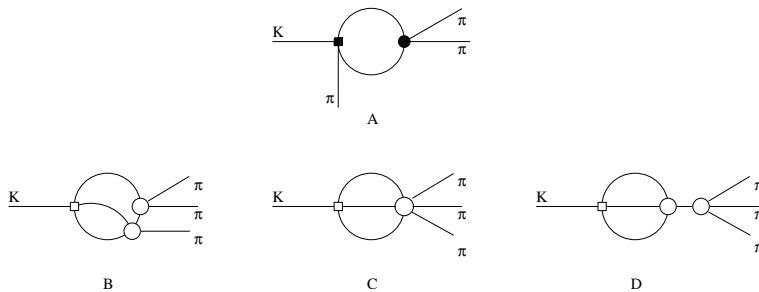


Figure 1: Some topologies contributing to the FSI in $K \rightarrow 3\pi$ decays at LO and NLO. The square is the weak vertex and the circle is the strong one. In topology A, solid circles include both tree and one-loop level vertices.

$K \rightarrow 3\pi$ amplitudes including isospin breaking effects from quark masses and electromagnetic interactions [12, 13].

In the mean time, we discovered some small errata in the published formulas in [5] which were corrected in [6]. We correct here another erratum in Eqs. (6.6), (6.7) and (6.9) in [5] where we wrote \mathbb{R} instead of $\tilde{\mathbb{R}}$. See Section 3 in the present work for the correction. In addition, the matrix elements 21 and 22 in Eqs. (6.7) and (6.9) in [5] were interchanged. None of these errata affects the results for the CP-violating asymmetries nor the conclusions given in [5, 6, 7].

The details of the use of the optical theorem to calculate the two-pion cut contributions of topology A in Figure 1 –solid circles include both tree and one-loop level vertices– were given in Appendix E of the first reference in [5]. Notice that two-pion cuts of topology B are already included in topology A when one takes the weak vertex at one-loop. We don’t repeat them now.

Here, we complete the calculation of these FSI by evaluating the three-pion cuts in topologies B, C and D in Figure 1 for $K^+ \rightarrow 3\pi$. We also provide with the neutral kaon $K_{L,S} \rightarrow 3\pi$ final state interactions at $\mathcal{O}(p^6)$ including both from two- and three-pion cuts. Thus, we give the full $K \rightarrow 3\pi$ FSI at NLO in CHPT in the isospin limit for all $K \rightarrow 3\pi$ decays.

The study of FSI in $K \rightarrow 3\pi$ at two-loops also became of relevance after the proposal by Cabibbo [14] to measure the combination $a_0 - a_2$ of $\pi\pi$ scattering lengths using the cusp effect in the $\pi^0\pi^0$ spectrum at threshold in $K^+ \rightarrow \pi^+\pi^0\pi^0$ and $K_L \rightarrow \pi^0\pi^0\pi^0$ decay rates. Within this proposal, it has been recently presented in [15] the effects of FSI at NLO using formulas dictated by unitarity and analyticity approximated at second order in the $\pi\pi$ scattering lengths, $a_i \sim 0.2$. The error was therefore canonically assumed to be of order of a_i^2 , i.e., 5%. It is of interest to check this canonical error and provide a complementary analysis of the theoretical uncertainty. We use our NLO in CHPT results for the form of the real part of $K \rightarrow 3\pi$ which has to be fitted to data to give the formulas of the cusp effect always leaving the $\pi\pi$ scattering near threshold as in Cabibbo’s original proposal. The advantage of using CHPT is that it contains the correct singularity structure at NLO in CHPT which can be systematically improved in an effective field theory framework by going at higher orders.

Contributions from next-to-next-to-leading order (NNLO) SU(3) CHPT in the isospin limit are expected typically to be around ($3 \sim 5$)%, so that our NLO results are just a first step in order to reduce the theoretical error on the determination of the combination $a_0 - a_2$ to the few per cent level. Once the isospin limit NNLO CHPT contribution is eventually evaluated, one can follow the procedure that we use here to get a more accurate measurement of $a_0 - a_2$ and check the assumed NNLO uncertainty. At that point, and in order to reach the few per cent level in the theoretical uncertainty, it will be necessary to include full isospin breaking effects at NLO too which are also expected to be of a few per cent as was found for $K \rightarrow 3\pi$ in [12, 13].

In Sections 2 and 3 we introduce the needed notation in the description of $K \rightarrow 3\pi$ in CHPT and the final state interactions at NLO, respectively. In Section 4 we give the relevant formulas using our NLO results for the singularity structure of the real part of $K \rightarrow 3\pi$ to be used in a fit of the experimental $K \rightarrow 3\pi$ cusp effect to data to extract the $a_0 - a_2$ phase shift combination. We compare our results with the ones in [15] and give estimates of the theoretical uncertainties in the determination of $a_0 - a_2$. We do this both for $K^+ \rightarrow \pi^+\pi^0\pi^0$ and for $K_L \rightarrow \pi^0\pi^0\pi^0$. Finally, we summarize our results and main conclusions in Section 5.

In Appendix A we list the numerical inputs used. In Appendix B we present the FSI results for the neutral kaon $K \rightarrow 3\pi$ decays from two-pion cut contributions to topology A in Figure 1. Finally, in Appendix C we collect the results for all three-pion cut contributions to topologies B, C, and D in Figure 1.

2. Notation

Here, we want to give the basic notation that we use in the following. In [5] we calculated the amplitudes with $K_{1(2)} \equiv \left(K^0 - (+)\overline{K^0} \right) / \sqrt{2}$,

$$\begin{aligned}
K_2(k) &\rightarrow \pi^0(p_1)\pi^0(p_2)\pi^0(p_3), & [A_{000}^2], \\
K_2(k) &\rightarrow \pi^+(p_1)\pi^-(p_2)\pi^0(p_3), & [A_{+-0}^2], \\
K_1(k) &\rightarrow \pi^+(p_1)\pi^-(p_2)\pi^0(p_3), & [A_{+-0}^1], \\
K^+(k) &\rightarrow \pi^0(p_1)\pi^0(p_2)\pi^+(p_3), & [A_{00+}], \\
K^+(k) &\rightarrow \pi^+(p_1)\pi^+(p_2)\pi^-(p_3), & [A_{++-}],
\end{aligned} \tag{2.1}$$

as well as their CP-conjugated decays at NLO (i.e. order p^4 in this case) in the chiral expansion and in the isospin symmetry limit $m_u = m_d$.

The lowest order SU(3) \times SU(3) chiral Lagrangian describing $|\Delta S| = 1$ transitions is

$$\begin{aligned}
\mathcal{L}_{|\Delta S|=1}^{(2)} &= C F_0^6 e^2 G_E \text{tr} \left(\Delta_{32} u^\dagger Q u \right) + C F_0^4 \left[G_8 \text{tr} \left(\Delta_{32} u_\mu u^\mu \right) + G_8' \text{tr} \left(\Delta_{32} \chi_+ \right) \right. \\
&\quad \left. + G_{27} t^{ij,kl} \text{tr} \left(\Delta_{ij} u_\mu \right) \text{tr} \left(\Delta_{kl} u^\mu \right) \right] + \text{h.c.}
\end{aligned} \tag{2.2}$$

with

$$C = -\frac{3}{5} \frac{G_F}{\sqrt{2}} V_{ud} V_{us}^* \simeq -1.07 \times 10^{-6} \text{ GeV}^{-2}. \tag{2.3}$$

The correspondence with the couplings c_2 and c_3 of [10] is

$$\begin{aligned} c_2 &= CF_0^4 G_8; \\ c_3 &= -\frac{1}{6}CF_0^4 G_{27}. \end{aligned} \quad (2.4)$$

F_0 is the chiral limit value of the pion decay constant $f_\pi = (92.4 \pm 0.4)$ MeV,

$$\begin{aligned} u_\mu &\equiv iu^\dagger(D_\mu U)u^\dagger = u_\mu^\dagger, \\ \Delta_{ij} &= u\lambda_{ij}u^\dagger \quad (\lambda_{ij})_{ab} \equiv \delta_{ia}\delta_{jb}, \\ \chi_{+(-)} &= u^\dagger\chi u^\dagger + (-)u\chi^\dagger u \end{aligned} \quad (2.5)$$

$\chi = \text{diag}(m_u, m_d, m_s)$ is a 3×3 matrix collecting the light quark masses, $U \equiv u^2 = \exp(i\sqrt{2}\Phi/F_0)$ is the exponential representation incorporating the octet of light pseudo-scalar mesons in the SU(3) matrix Φ ;

$$\Phi \equiv \begin{pmatrix} \frac{\pi^0}{\sqrt{2}} + \frac{\eta_8}{\sqrt{6}} & \pi^+ & K^+ \\ \pi^- & -\frac{\pi^0}{\sqrt{2}} + \frac{\eta_8}{\sqrt{6}} & K^0 \\ K^- & \bar{K}^0 & -2\frac{\eta_8}{\sqrt{6}} \end{pmatrix}.$$

The non-zero components of the SU(3) \times SU(3) tensor $t^{ij,kl}$ are

$$\begin{aligned} t^{21,13} &= t^{13,21} = \frac{1}{3}; \quad t^{22,23} = t^{23,22} = -\frac{1}{6}; \\ t^{23,33} &= t^{33,23} = -\frac{1}{6}; \quad t^{23,11} = t^{11,23} = \frac{1}{3}; \end{aligned} \quad (2.6)$$

and $Q = \text{diag}(2/3, -1/3, -1/3)$ is a 3×3 matrix which collects the electric charge of the three light quark flavors.

Making use of the Dalitz variables

$$x \equiv \frac{s_1 - s_2}{m_{\pi^+}^2} \quad \text{and} \quad y \equiv \frac{s_3 - s_0}{m_{\pi^+}^2} \quad (2.7)$$

with $s_i \equiv (k - p_i)^2$, $3s_0 \equiv m_K^2 + m_{\pi^{(1)}}^2 + m_{\pi^{(2)}}^2 + m_{\pi^{(3)}}^2$, the amplitudes in (2.1) [without isospin breaking terms] can be written as expansions in powers of x and y

$$\begin{aligned} A_{++-} &= (-2\alpha_1 + \alpha_3) - (\beta_1 - \frac{1}{2}\beta_3 + \sqrt{3}\gamma_3)y + \mathcal{O}(y^2, x), \\ A_{00+} &= \frac{1}{2}(-2\alpha_1 + \alpha_3) - (-\beta_1 + \frac{1}{2}\beta_3 + \sqrt{3}\gamma_3)y + \mathcal{O}(y^2, x), \\ A_{+-0}^2 &= (\alpha_1 + \alpha_3)^R - (\beta_1 + \beta_3)^R y + \mathcal{O}(y^2, x), \\ A_{+-0}^1 &= (\alpha_1 + \alpha_3)^I - (\beta_1 + \beta_3)^I y + \mathcal{O}(y^2, x), \\ A_{000}^2 &= 3(\alpha_1 + \alpha_3)^R + \mathcal{O}(y^2, x), \\ A_{000}^1 &= 3(\alpha_1 + \alpha_3)^I + \mathcal{O}(y^2, x), \end{aligned} \quad (2.8)$$

where the parameters α_i , β_i and γ_i are functions of the pion and kaon masses, F_0 , the lowest order $\Delta S = 1$ Lagrangian couplings G_8 , G'_8 , G_{27} , G_E and the counterterms appearing at order p^4 , i.e., $L'_i s$ and $\tilde{K}'_i s$. The definition of these last ones can be found in Section 3.2 of [5]. In (2.8), super-indices R and I mean that either the real or the imaginary part of the counterterms appear.

If we do not consider FSI, the complex parameters α_i , β_i and γ_i can be written at NLO in terms of the order p^2 and p^4 counterterms and the constants $B_{i,0(1)} = B_{i,0(1)}^{(2)} + B_{i,0(1)}^{(4)}$ and $H_{i,0(1)}^{(4)}$ defined in Appendix B of [5]. There, we gave α_i , β_i and γ_i at LO in CHPT as well as their analytic expressions at NLO.

3. FSI for $K \rightarrow 3 \pi$ at NLO

The strong FSI mix the two final states with isospin $I = 1$ and leave unmixed the isospin $I = 2$ state. The mixing in the isospin $I = 1$ decay amplitudes is taken into account by introducing the strong re-scattering 2×2 matrix \mathbb{R} . The amplitudes in (2.1) including the FSI effects can be written at all orders, in the isospin symmetry limit, as follows [16],

$$\begin{aligned} T_c \begin{pmatrix} A_{++-}^{(I=1)} \\ A_{00+}^{(I=1)} \end{pmatrix}_{\text{Res}} &= (\mathbb{I} + i \mathbb{R}) T_c \begin{pmatrix} A_{++-}^{(I=1)} \\ A_{00+}^{(I=1)} \end{pmatrix}_{\text{NRes}} , \\ T_n \begin{pmatrix} A_{+-0}^2 \\ A_{000}^2 \end{pmatrix}_{\text{Res}} &= (\mathbb{I} + i \mathbb{R}) T_n \begin{pmatrix} A_{+-0}^2 \\ A_{000}^2 \end{pmatrix}_{\text{NRes}} , \\ A_{++-}^{(I=2)}|_{\text{Res}} &= (1 + i \delta_2) A_{++-}^{(I=2)}|_{\text{NRes}} , \end{aligned} \tag{3.1}$$

with the matrices

$$T_c = \frac{1}{3} \begin{pmatrix} 1 & 1 \\ 1 & -2 \end{pmatrix} , \quad T_n = \frac{1}{3} \begin{pmatrix} 0 & 1 \\ -3 & 1 \end{pmatrix} \tag{3.2}$$

projecting the final state with $I = 1$ into the symmetric–non-symmetric basis [16]. The subscript Res (NRes) in (3.1) means that the re-scattering effects have (not) been included. In these definitions, the matrix \mathbb{R} , δ_2 and the amplitudes $A^{(i)}$ depend on s_1 , s_2 and s_3 .

Using the usual isospin decomposition of $K \rightarrow 3\pi$ amplitudes in the isospin limit

$$\begin{aligned} A_{++-}(s_1, s_2, s_3) &= 2A_c(s_1, s_2, s_3) + B_c(s_1, s_2, s_3) + B_t(s_1, s_2, s_3) , \\ A_{00+}(s_1, s_2, s_3) &= A_c(s_1, s_2, s_3) - B_c(s_1, s_2, s_3) + B_t(s_1, s_2, s_3) , \\ A_{+-0}(s_1, s_2, s_3) &= C_0(s_1, s_2, s_3) + \frac{2}{3} [B_t(s_3, s_2, s_1) - B_t(s_3, s_1, s_2)] \\ &\quad + A_n(s_1, s_2, s_3) - B_n(s_1, s_2, s_3) , \\ A_{000}(s_1, s_2, s_3) &= 3A_n(s_1, s_2, s_3) , \end{aligned} \tag{3.3}$$

one finds for the elements of \mathbb{R} ,

$$\mathbb{R}_{11} = \frac{B_n^{\text{NRes}} \text{Im} A_c - B_c^{\text{NRes}} \text{Im} A_n}{A_c^{\text{NRes}} B_n^{\text{NRes}} - A_n^{\text{NRes}} B_c^{\text{NRes}}} ,$$

$$\begin{aligned}
\mathbb{R}_{12} &= \frac{A_c^{\text{NRes}} \text{Im} A_n - A_n^{\text{NRes}} \text{Im} A_c}{A_c^{\text{NRes}} B_n^{\text{NRes}} - A_n^{\text{NRes}} B_c^{\text{NRes}}}, \\
\mathbb{R}_{21} &= \frac{B_n^{\text{NRes}} \text{Im} B_c - B_c^{\text{NRes}} \text{Im} B_n}{A_c^{\text{NRes}} B_n^{\text{NRes}} - A_n^{\text{NRes}} B_c^{\text{NRes}}}, \\
\mathbb{R}_{22} &= \frac{A_c^{\text{NRes}} \text{Im} B_n - A_n^{\text{NRes}} \text{Im} B_c}{A_c^{\text{NRes}} B_n^{\text{NRes}} - A_n^{\text{NRes}} B_c^{\text{NRes}}}.
\end{aligned} \tag{3.4}$$

At LO, $\mathbb{R}_{12} = 0$ due to the fact that the only contributions to $\text{Im}A_i$ come from $\pi\pi$ re-scattering. At higher orders there are contributions to $\text{Im}A_i$ which have different origin and therefore $\mathbb{R}_{12} \neq 0$. Notice that the re-scattering matrix \mathbb{R} depends on energy and at $\pi\pi$ threshold it changes –this is in fact the cusp effect discussed in the following sections.

As explained in [5], we used the optical theorem to calculate the two-pion cuts contributions to FSI at NLO for the charged kaon decays which are the dominant ones. The analytical result of these contributions for the dispersive part of the amplitudes for $K^+ \rightarrow 3\pi$ can be found in Appendix E of the first reference in [5]. Here, we also calculate analytically these contributions to FSI at NLO for all $K_{L,S} \rightarrow 3\pi$ and include the three-pion cut contributions in topologies B and C in Figure 1 in all cases. These last three-pion cut contributions have been evaluated numerically –see Appendix C.

The calculation has been done in the isospin limit, apart of the kinematical factors in the optical theorem. This constitutes the first full calculation of FSI in $K \rightarrow 3\pi$ decays at NLO in CHPT. The results for the dispersive part of the amplitudes for $K_{L,S} \rightarrow 3\pi$ can be found in Appendix B for two-pion cuts and in Appendix C for three-pion cuts for both neutral and charged $K \rightarrow 3\pi$. For the numerical applications in the rest of the paper, we use the inputs in Appendix A.

Equations (3.1) imply the following relation for the two first coefficients of the expansion in powers of x and y of the amplitudes in (2.8)

$$\begin{aligned}
\begin{pmatrix} -\alpha_1 + \frac{1}{2}\alpha_3 \\ -\beta_1 + \frac{1}{2}\beta_3 \end{pmatrix}_{\text{Res}} &= \left(\mathbb{I} + i \widetilde{\mathbb{R}} \right) \begin{pmatrix} -\alpha_1 + \frac{1}{2}\alpha_3 \\ -\beta_1 + \frac{1}{2}\beta_3 \end{pmatrix}_{\text{NRes}}, \\
\begin{pmatrix} \alpha_1 + \alpha_3 \\ \beta_1 + \beta_3 \end{pmatrix}_{\text{Res}} &= \left(\mathbb{I} + i \widetilde{\mathbb{R}} \right) \begin{pmatrix} \alpha_1 + \alpha_3 \\ \beta_1 + \beta_3 \end{pmatrix}_{\text{NRes}}, \\
\gamma_{3,\text{Res}} &= (1 + i \delta_2) \gamma_{3,\text{NRes}}.
\end{aligned} \tag{3.5}$$

The matrix $\widetilde{\mathbb{R}}$ and the phase δ_2 were given at LO in [5]. We also gave there the two combinations of the $\widetilde{\mathbb{R}}$ matrix elements that can be obtained from the charged kaon decays. As we already said in the Introduction, there is an erratum in Eqs. (6.6), (6.7) and (6.9) in [5] where we wrote \mathbb{R} instead of $\widetilde{\mathbb{R}}$. In addition, in Eqs. (6.7) and (6.9) the matrix elements 21 and 22 were interchanged.

4. Cabibbo's Proposal at NLO in CHPT

Recently, Cabibbo [14] showed that the cusp effect in the total energy spectrum of the

$\pi^0\pi^0$ pair in $K^+ \rightarrow \pi^+\pi^0\pi^0$ is proportional to the scattering lengths combination $a_0 - a_2$ and proposed to use this effect to measure it.

This interesting proposal was done at lowest order in the sense that the author just considered topologies of type A in Figure 1. It has been followed up by a study of higher order re-scattering effects coming from topology B in Figure 1 [15]. The first experimental analysis applying this proposal has been already published in [17] showing clearly that the nominal 5 % theoretical accuracy quoted in [15] will dominate this determination. It is therefore very important to check this 5% theoretical uncertainty and how to reduce it further.

In [15], in order to make a quantitative evaluation for the Cabibbo's proposal uncertainties, a power counting in the scattering lengths a_i was done. The main conclusion was that one needs to include topology B in Figure 1 to go to $\mathcal{O}(a^2)$ accuracy, i.e. around 5%. The authors used Feynman diagrammatics to do the counting in powers of a_i although at present there is no effective field theory supporting it. It is of course interesting to construct it and follow that program. In [14, 15], the real part of the $K \rightarrow 3\pi$ amplitude was approximated by a second order polynomial in the relevant final two-pion invariant energy which is fitted to data. We believe that it is also interesting to study the Cabibbo's proposal using the exact form at NLO in CHPT for the real part of $K \rightarrow 3\pi$ also fitted to data. We present this analysis below. We anticipate that our proposal uses exact NLO CHPT results but is not just full CHPT at that order. In that respect, it is a variation of the original Cabibbo's proposal that uses NLO CHPT for the real part of $K \rightarrow 3\pi$ vertex instead of the polynomial approximation used in [14, 15] and the optical theorem.

The cusp effect originates in the different contributions of $\pi\pi$ scattering to the $K^+ \rightarrow \pi^+\pi^0\pi^0$ and $K_L^0 \rightarrow \pi^0\pi^0\pi^0$ amplitudes above and below threshold of $\pi^+\pi^-$ production. In Section 4.1 for $K^+ \rightarrow \pi^+\pi^0\pi^0$ and in Section 4.2 for $K^0 \rightarrow \pi^0\pi^0\pi^0$, we obtain these contributions using just analyticity and unitarity, i.e. applying the optical theorem above or below threshold. In some cases going below threshold becomes unphysical because the value of the real world pion masses forbids it. In such cases we follow the strategy in [15] of going first to unphysical value of pion masses, e.g. $m_{\pi^0} > m_{\pi^+}$, such that the absorptive part below threshold exists and apply the optical theorem in this set up. Then the result is analytically continued above threshold where the amplitude always exists by putting the real value for pion masses.

The explicit application of the optical theorem to $K \rightarrow 3\pi$ with physical thresholds can be found in [5] and has been used in the previous section. The optical theorem allows to separate the $\pi\pi$ scattering in the final state interactions, i.e the scattering length effects, from the rest in $K \rightarrow 3\pi$. In particular, we introduce the real part of $\pi\pi$ scattering near threshold in the optical theorem non-perturbatively. This means that as the effect of the $\pi\pi$ scattering must be estimated around threshold, one is intuitively lead to use the scattering length to all orders as a good approximation of $\pi\pi$ scattering in the optical theorem.

Explicitly, we follow [14, 15] for the treatment of $\pi\pi$ scattering matrix elements near threshold. At threshold, we use [4]

$$\pi^0\pi^0 \rightarrow \pi^0\pi^0, \quad \text{Re } A_{00} \equiv 32\pi a_{00} \quad \text{with} \quad a_{00} = \frac{a_0 + 2a_2}{3},$$

$$\begin{aligned}
\pi^+\pi^0 \rightarrow \pi^+\pi^0, & \quad \text{Re } A_{+0} \equiv 32\pi a_{+0} & \quad \text{with} & \quad a_{+0} = \frac{a_2}{2}, \\
\pi^+\pi^- \rightarrow \pi^0\pi^0, & \quad \text{Re } A_x \equiv 32\pi a_x & \quad \text{with} & \quad a_x = \frac{a_0 - a_2}{3}, \\
\pi^+\pi^- \rightarrow \pi^+\pi^-, & \quad \text{Re } A_{+-} \equiv 32\pi a_{+-} & \quad \text{with} & \quad a_{+-} = \frac{2a_0 + a_2}{3}, \\
\pi^+\pi^+ \rightarrow \pi^+\pi^+, & \quad \text{Re } A_{++} \equiv 32\pi a_{++} & \quad \text{with} & \quad a_{++} = a_2,
\end{aligned} \tag{4.1}$$

as a definition of the different effective scattering length combinations measured by fitting the measured cusp effect. We take their expressions in terms of a_0 and a_2 in the isospin conserving limit only as a first approximation. The quantities determined experimentally for these effective scattering lengths combinations should be compared with the CHPT prediction including radiative corrections and isospin breaking [15]. Notice that the scattering lengths are defined at the following thresholds s_{th} : $4m_{\pi^+}^2$ for a_{00} , a_x , a_{+-} and a_{++} and $(m_{\pi^+} + m_{\pi^0})^2$ for a_{+0} .

In order to describe the $\pi\pi$ scattering away from threshold one should take into account the kinematical dependence of the amplitudes. Whenever an amplitude is centered around threshold, we follow [15] and perform an expansion in the different kinematical variables on which the amplitudes depend. Up to linear terms, the generic matrix elements –neglecting all higher order but the P wave– are of the form [18]

$$\text{Re } A_{ij} = 32\pi \left[a_{ij}(s) + \frac{3}{4} a_{ij}^P \frac{(t-u)}{m_{\pi^+}^2} \right] \tag{4.2}$$

with²

$$a_{ij}(s) = a_{ij} \left[1 + r_{ij} \frac{(s - s_{th})}{4m_{\pi^+}^2} \right] \tag{4.3}$$

where $a_{ij}(s)$ are the ones defined in (4.1) but with $a_0(s)$ and $a_2(s)$. For numerical applications, we use $r_0 = 1.25 \pm 0.04$ and $r_2 = 1.81 \pm 0.05$ [18] which are compatible with the results in [19] and

$$a_{+-}^P = a_{+0}^P = a_1/2 \tag{4.4}$$

with $a_1^{CHPT} = m_\pi^2/(12\pi F_0^2)$ to lowest order in CHPT. The rest of a_{ij}^P are zero.

The above discussion fixes the real part of $\pi\pi$ amplitudes to be used in the optical theorem when they are evaluated near threshold. Whenever $\pi\pi$ amplitudes are evaluated very far from threshold (say $s \sim m_K^2$) we use full NLO CHPT expressions.

For the other ingredient needed in the optical theorem –the real part of $K \rightarrow 3\pi$ amplitudes– the procedure we propose to take into account the re-scattering effects in a systematically improvable manner is to treat it perturbatively within CHPT, i.e., first at tree-level (LO), next at one-loop (NLO), \dots . This is the main point of this analysis and the difference with the approach in [15]. It is the first step to go to NNLO and reduce the theoretical uncertainty to the percent level.

²The effects of $\pi\pi$ threshold singularities are NNLO in a chiral counting and expected to be small. However one should include them since as we said we want to treat the $\pi\pi$ scattering non-perturbatively –this can be done as in [15].

Notice that the use of the CHPT formula for the real part of $K \rightarrow 3\pi$ does not change the need of fitting it to data. The aim is *not* to predict the real part of $K \rightarrow 3\pi$ but to describe its analytic structure as accurately as possible so that, once separated the real part of $K \rightarrow 3\pi$ from $\pi\pi$ scattering through the optical theorem, one can measure $\pi\pi$ scattering near threshold as Cabibbo proposed. In particular, $\pi\pi$ scattering near threshold is treated non-perturbatively as proposed in [14]. The advantage now is that we have the correct structure of singularities at a given CHPT order for real part of $K \rightarrow 3\pi$ and this can be improved systematically. Below we give the cusp effect formulas within this approach.

4.1 Cabibbo's Proposal for Charged Kaon Decays

We can decompose the $K^+ \rightarrow \pi^+\pi^0\pi^0$ amplitude in the following way according to [15]

$$A_{00+} = \begin{cases} \bar{A}_{00+} + \bar{B}_{00+}v_{\pm}(s_3), & s_3 > 4m_{\pi^+}^2, \\ \bar{A}_{00+} + i\bar{B}_{00+}v_{\pm}(s_3), & s_3 < 4m_{\pi^+}^2, \end{cases} \quad (4.5)$$

where \bar{A}_{00+} and \bar{B}_{00+} are regular functions except at the $\pi^+\pi^-$ threshold and

$$v_{ij}(s) = \sqrt{\frac{|s - (m_{\pi_i} + m_{\pi_j})^2|}{s}}. \quad (4.6)$$

With these definitions, the differential decay rate for this amplitude can be written as [15]

$$|A_{00+}|^2 \equiv \text{Re}\bar{A}_{00+}^2 + \Delta_A + v_{\pm}(s_3)\Delta_{\text{cusp}}, \quad (4.7)$$

with

$$\Delta_A \equiv \text{Im}\bar{A}_{00+}^2 + v_{\pm}^2(s_3) \left[\text{Re}\bar{B}_{00+}^2 + \text{Im}\bar{B}_{00+}^2 \right], \quad (4.8)$$

$$\Delta_{\text{cusp}} \equiv \begin{cases} -2\text{Re}\bar{A}_{00+}\text{Im}\bar{B}_{00+} + 2\text{Im}\bar{A}_{00+}\text{Re}\bar{B}_{00+}, & s_3 < 4m_{\pi^+}^2 \\ 2\text{Re}\bar{A}_{00+}\text{Re}\bar{B}_{00+} + 2\text{Im}\bar{A}_{00+}\text{Im}\bar{B}_{00+}, & s_3 > 4m_{\pi^+}^2. \end{cases} \quad (4.9)$$

The combination of real and imaginary amplitudes Δ_{cusp} defined above parametrizes the cusp effect due to the $\pi^+\pi^- \rightarrow \pi^0\pi^0$ re-scattering in the $K^+ \rightarrow \pi^+\pi^0\pi^0$ decay rate, taking different values above and below the threshold $s_3 = 4m_{\pi^+}^2$ associated to this re-scattering.

At this level, we can use the real part of A_{00+} result at one-loop in CHPT to fit data. We use it in the following. This provides a fit at least as good as the second order polynomial parametrization used in the original proposal [14, 15] and its precision is just limited by data and the singularity structure at NLO in CHPT.

The absorptive part of A_{00+} is

$$\text{Im}A_{00+} = \begin{cases} \text{Im}\bar{A}_{00+} + \text{Im}\bar{B}_{00+}v_{\pm}(s_3), & s_3 > 4m_{\pi^+}^2, \\ \text{Im}\bar{A}_{00+} - \text{Re}\bar{B}_{00+}v_{\pm}(s_3), & s_3 < 4m_{\pi^+}^2. \end{cases} \quad (4.10)$$

We calculate the absorptive part above threshold in (4.10) using the optical theorem, where we consistently use the NLO expression for $\text{Re}A_{00+}$ fitted to data. The application of the optical theorem below threshold for unphysical pion masses $m_{\pi^0} > m_{\pi^+}$ produces the same result for $\text{Re}\bar{B}_{00+}$ as the real world pion masses one.

Notice that the accuracy with which we predict the cusp can be improved systematically by going at higher order in the loop expansion, which produces a more accurate singularity structure. The real part of the amplitude $K^+ \rightarrow \pi^+\pi^0\pi^0$, i.e. $\text{Re } \bar{A}_{00+}$, was calculated at NLO in CHPT in the isospin limit in [5, 9]. While the two-pion cut contributions to its dispersive part were calculated analytically at two-loops in [5] as explained in Section 3. The rest of the NLO contributions to the dispersive part of A_{00+} correspond to the three-pion cuts in topologies B, C and D in Figure 1 which are expected to be very small. They have been calculated here numerically for completeness and checked that they are negligible (see Appendix C for the results). They can be safely disregarded and we do not include them in our cusp effect formulas.

With those results at hand, we can study the scattering lengths combination $a_0 - a_2$ determination from (4.9) using the NLO CHPT formulas for the real part of the $K^+ \rightarrow \pi^+\pi^0\pi^0$ vertex in the optical theorem as explained above. For the real part of $\pi^+\pi^-\pi^0 \rightarrow \pi^0\pi^0$ scattering we use the non-perturbative definition explained in Section 4. First, we give the expressions for the functions \bar{A}_{00+} and \bar{B}_{00+} using the tree-level CHPT expression to fit the real part of $K^+ \rightarrow \pi^+\pi^0\pi^0$ to data, we get

$$\begin{aligned}
\text{Re}\bar{A}_{00+}|_{LO} &= C' \left[\text{Re } G_8(m_\pi^2 - s_3) + G_{27} \frac{1}{16(m_K^2 - m_\pi^2)} [s_3(4m_\pi^2 - 19m_K^2) + \right. \\
&\quad \left. + 5m_K^4 - 4m_\pi^4 + 19m_K^2 m_\pi^2] \right], \\
\text{Im}\bar{A}_{00+}|_{LO} &= C' \left[-v_{00}(s_3)a_{00}(s_3) \left[\text{Re } G_8(s_3 - m_\pi^2) + G_{27} \frac{1}{6(m_K^2 - m_\pi^2)} \times \right. \right. \\
&\quad \left. \left. \times (4m_\pi^4 - 5m_K^4 - 19m_\pi^2 m_K^2 - s_3(4m_\pi^2 - 19m_K^2)) \right] + \right. \\
&\quad \left. + [v_{+0}(s_1)(SW_{+0}^{LO}(s_1) + (s_2 - s_3)PW_{+0}^{LO}(s_1)) + s_1 \leftrightarrow s_2] \right], \\
SW_{+0}^{LO}(s) &= \frac{(s - 2m_\pi^2)}{64\pi f_\pi^2} \left[\text{Re } G_8(m_K^2 + m_\pi^2 - s) + \frac{G_{27}}{6(m_K^2 - m_\pi^2)} (9m_K^4 + \right. \\
&\quad \left. + m_K^2(15m_\pi^2 - 19s) + 4m_\pi^2(s - m_\pi^2)) \right] \\
PW_{+0}^{LO}(s) &= \frac{(s - 4m_\pi^2)}{192\pi f_\pi^2} \left[\text{Re } G_8 + \frac{G_{27}}{6(m_K^2 - m_\pi^2)} (19m_K^2 - 4m_\pi^2) \right], \\
\text{Re}\bar{B}_{00+}|_{LO} &= 0, \\
\text{Im}\bar{B}_{00+}|_{LO} &= C' a_x(s_3) \left[-\text{Re } G_8(s_3 - m_\pi^2 + m_K^2) + G_{27} \frac{1}{3} [13s_3 - 7m_K^2 - 13m_\pi^2] \right] (4.11)
\end{aligned}$$

where $C' = iC F_0^4 / (f_\pi^3 f_K)$ and the constant C is defined in (2.3). Notice that LO here does not mean fully LO in CHPT. We have consistently used the LO CHPT expression to fit $\text{Re}\bar{A}_{00+}$, which is dispersive, while $\text{Im}A_{00+}$ and $\text{Im}\bar{B}_{00+}$ which are absorptive are taken at $\mathcal{O}(p^4)$. Since $\text{Re}\bar{B}_{00+}$ is obtained below threshold where it is absorptive, one has to take it at $\mathcal{O}(p^4)$. We are always treating the $\pi\pi$ scattering lengths to all orders.

Using the CHPT expression up to one-loop [5, 9] to fit the real part of $K^+ \rightarrow \pi^+\pi^0\pi^0$

to data, we get

$$\begin{aligned}
\text{Re}\bar{A}_{00+}|_{NLO} &= \text{Re}\bar{A}_{00+}|_{LO} + [M_7(s_3) + M_8(s_1) + M_8(s_2) + M_9(s_1)(s_2 - s_3) + \\
&\quad + M_9(s_2)(s_1 - s_3)]|_{\mathcal{O}(p^4)}, \\
\text{Im}\bar{A}_{00+}|_{NLO} &= \text{Im}\bar{A}_{00+}|_{LO} + v_{00}(s_3)a_{00}(s_3) \left[M_7(s_3) + \widetilde{M}_8(s_3) + \right. \\
&\quad \left. + \widetilde{M}_9(s_3)(m_K^2 + 3m_\pi^2 - 2s_3) - \widetilde{M}_9^s(s_3) \right] |_{\mathcal{O}(p^4)} + \\
&\quad + \left[v_{+0}(s_1)(SW_{+0}^{NLO}(s_1) + (s_2 - s_3)PW_{+0}^{NLO}(s_1)) + s_1 \leftrightarrow s_2 \right], \\
\text{Re}\bar{B}_{00+}|_{NLO} &= -v_{00}(s_3) \left[a_{00}(s_3)\text{Im}\bar{B}_{00+} + 2a_x(s_3)^2\text{Re}\bar{A}_{00+} \right], \\
\text{Im}\bar{B}_{00+}|_{NLO} &= \text{Im}\bar{B}_{00+}|_{LO} + a_x(s_3) \left[2M_{11}(s_3) + \widetilde{M}_{10}(s_3) + \widetilde{M}_{11}(s_3) - \right. \\
&\quad \left. - \widetilde{M}_{12}(s_3)(m_K^2 + 3m_\pi^2 - 2s_3) + \widetilde{M}_{12}^s(s_3) \right] |_{\mathcal{O}(p^4)}, \tag{4.12}
\end{aligned}$$

where we have neglected the three-pion cut graph contributions as explained above. Again, here NLO does not mean fully NLO in CHPT. We have consistently used the NLO CHPT expression to fit $\text{Re}\bar{A}_{00+}$ which we are treating perturbatively while we are always treating the $\pi\pi$ scattering lengths to all orders. We are applying a chiral counting just to the $K^+ \rightarrow \pi^+\pi^0\pi^0$ vertex.

The contributions $SW_{+0}^{NLO}(s_1)$ and $PW_{+0}^{NLO}(s_1)$ were already calculated in [5] (the substitution $\sigma(s_i) \rightarrow v_\pm(s_i)$ in the formulas of [5] is understood),

$$\begin{aligned}
v_{+0}(s_1)SW_{+0}^{NLO}(s_1) + s_1 \leftrightarrow s_2 &= \text{formulas E.25} + \text{E.29 of [5]}, \\
v_{+0}(s_1)(s_2 - s_3)PW_{+0}^{NLO}(s_1) + s_1 \leftrightarrow s_2 &= \text{formulas E.26} + \text{E.30 of [5]}. \tag{4.13}
\end{aligned}$$

The functions $M_i(s)$ used in (4.12) are the same functions defined in [9] at order p^4 but exchanging the functions $B(m_\pi, m_\pi, s_3)$ there by

$$\mathcal{B}(m_\pi, m_\pi, s_3) = \mathcal{J}(m_\pi, s_3) - \frac{1}{16\pi^2} \left[\log \left(\frac{m_\pi^2}{\nu^2} \right) + 1 \right] \tag{4.14}$$

with

$$\mathcal{J}(m_\pi, s_3) = \frac{1}{16\pi^2} \begin{cases} 2 + v(s_3) \log \left(\frac{1-v(s_3)}{1+v(s_3)} \right) & s_3 > 4m_{\pi^+}^2 \\ 2 + 2v(s_3) \arctan v(s_3) & s_3 < 4m_{\pi^+}^2 \end{cases}$$

and $v = \sqrt{|s - 4m_\pi^2|/s}$. Functions \widetilde{M}_i and \widetilde{M}_i^s are defined in in Equation (B.1) in terms of the M_i functions.

At this point we would like to point out that we do not find the contributions $\text{Re}\bar{B}_{00+}$ above threshold analogous to those in Equation (4.28) of [15] nor the contribution to $\text{Re}\bar{A}_{00+}$ analogous to the one in Equation (4.3) in the same reference. They appear to come from an application of Cutkowsky rules beyond unitarity and analyticity and can only be checked with a full two-loop calculation of $K^+ \rightarrow \pi^+\pi^0\pi^0$. Going to any unphysical pion masses configuration and applying the optical theorem for topology C in Figure 1 does not produce those terms since they appear when $\pi^+\pi^- \rightarrow \pi^0\pi^0$ is below threshold which is not physical for any value of pion masses.

The relative effect of the cusp in $|A_{00+}|^2$ can be seen in Figure 2 where we plot $\frac{d|\Gamma_{\text{cusp}}(s_3)|}{ds_3}$ over $\frac{d\Gamma(s_3)}{ds_3}$ using the results in (4.12). Here, Γ_{cusp} is the contribution of $v_{\pm}(s_3)\Delta_{\text{cusp}}(s_1, s_3)$ in (4.9) to the total $K^+ \rightarrow \pi^+\pi^0\pi^0$ decay rate Γ ,

$$\frac{d\Gamma_{\text{cusp}}(s_3)}{ds_3} = \frac{1}{N} \int_{s_{1\text{min}}}^{s_{1\text{max}}} ds_1 v_{\pm}(s_3) \Delta_{\text{cusp}}(s_1, s_3), \quad (4.15)$$

where $N = 512\pi^3 m_K^3$, and $s_{1\text{max}}$ and $s_{1\text{min}}$ can be found in Eq. (4.4) of [5].

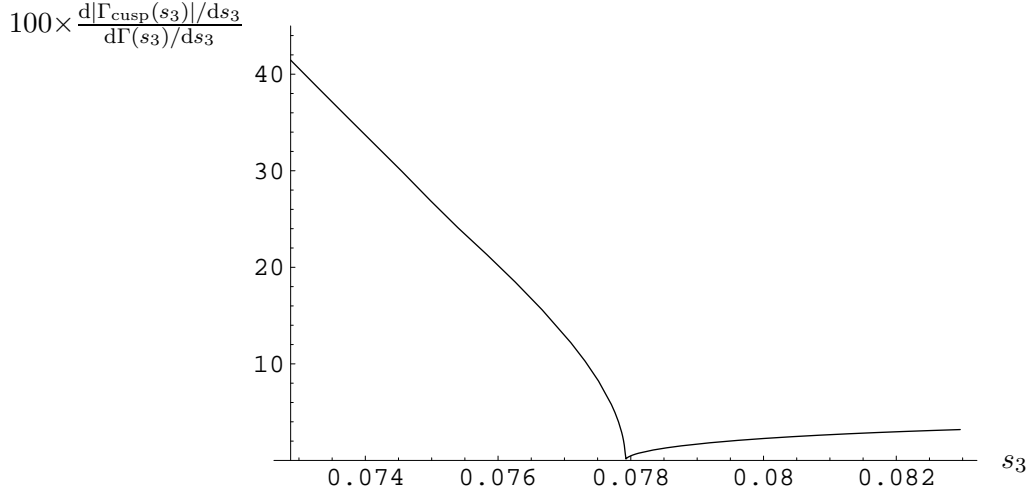


Figure 2: Plot of $100 \times \frac{d|\Gamma_{\text{cusp}}(s_3)|}{ds_3}$ over $\frac{d\Gamma(s_3)}{ds_3}$ around threshold as a function of s_3 , $4m_{\pi^0}^2 < s_3 < 4(2m_{\pi^+}^2 - m_{\pi^0}^2)$, for the decay $K^+ \rightarrow \pi^+\pi^0\pi^0$.

In Figure 3, we show the cusp effect for $K^+ \rightarrow \pi^+\pi^0\pi^0$ at NLO. The solid line is the

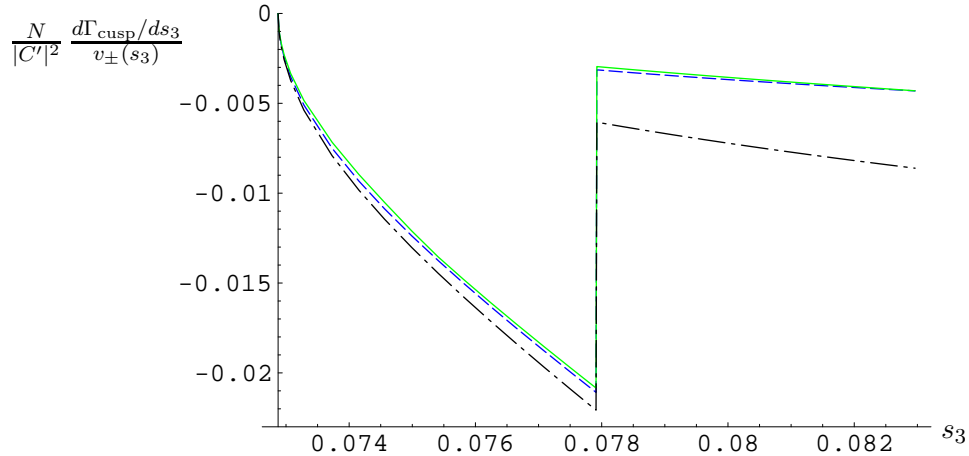


Figure 3: Plot of $\frac{N}{|C'|^2} \frac{d\Gamma_{\text{cusp}}/ds_3}{v_{\pm}(s_3)}$ around threshold as a function of s_3 , $4m_{\pi^0}^2 < s_3 < 4(2m_{\pi^+}^2 - m_{\pi^0}^2)$, for the decay $K^+ \rightarrow \pi^+\pi^0\pi^0$. The meaning of the various lines is explained in the text.

result for $\frac{N}{|C'|^2} \frac{d\Gamma_{\text{cusp}}/ds_3}{v_{\pm}(s_3)}$. The $\pi\pi$ scattering lengths are unknowns to be fixed by fitting the

cusplike effect, however for numerical comparison we take them as inputs given by CHPT [18] at NLO. For the rest of inputs needed for $\text{Re}\bar{A}_{00+}$ we use the ones in Appendix A which have been obtained from a fit to data.

Using the same value of the input $\pi\pi$ scattering lengths, we also plot $\frac{N}{|C'|^2} \frac{d\Gamma_{\text{cusp}}/ds_3}{v_{\pm}(s_3)}$ in Figure 3, as obtained using the results in [15] –this is the dot-dashed curve. For the slopes needed in $\text{Re}A_{00+}$ in (4.6) in [15] we use the Taylor expansion of our results for $|\text{Re}A_{00+}|^2 + |\text{Im}A_{00+}|^2$. We have also plotted the results in [15] without the contributions to $\text{Re}\bar{B}_{00+}$ and to $\text{Re}\bar{A}_{00+}$ above threshold that we do not find as explained above –this is the dashed curve. In this case, for the sake of a clearer comparison with the solid curve, we use the Taylor expansion of our results for $\text{Re}A_{00+}$ to get the slopes needed in (4.6) in [15].

If one compares now the dashed curve with the solid one, one gets differences both below and above threshold that vary between 5 % and 0. The piece $\text{Im}\bar{A}_{00+} \text{Re}\bar{B}_{00+}$ which is nominally order a^3 contributes less than 1 %. This provides a first handle on the theoretical uncertainty of the Cabibbo’s approach to obtain the scattering lengths since the differences between our approach and the one in [15] do not affect the treatment of the $\pi\pi$ scattering part. These numerical differences are just due to the analytic form of $\text{Re}\bar{A}_{00+}$ –either a quadratic polynomial for s_3 in [15] or the NLO in CHPT result here.

The difference between dashed and dot-dashed curves is around 5 % below threshold while above threshold is around 65 %. This difference has a twofold origin. One is the pieces that we do not find for $\text{Re}\bar{B}_{00+}$ above threshold. The other one is using the slopes in (4.6) in [15] from Taylor expanding $|\text{Re}A_{00+}|^2 + |\text{Im}A_{00+}|^2$ instead of $\text{Re}\bar{A}_{00+}$. This last effect amounts to 2.5 % below threshold and 1 % above threshold.

Above threshold, Δ_{cusp} is very sensitive to $\text{Re}\bar{B}_{00+}$ and the difference due to the contributions to $\text{Re}\bar{B}_{00+}$ that we do not find is much larger. The existence of these pieces is therefore an important issue.

There are other sources of theoretical uncertainties. For instance, the fit to experiment. In the case of using the CHPT NLO formulas for $\text{Re}\bar{A}_{00+}$, this fit produces central values of A_{00+} which agree with experiment within 3% accuracy [5, 9]. This global fit was done using total decay rates and Dalitz variable slopes. If one just used the data around threshold to make the fit, the accuracy would probably be at the 1% level or better. This uncertainty just measures how good is the fit of NLO CHPT formulas to experiment.

The source of uncertainty which is more difficult to estimate and that is present in any approach which describes the cusp effect to NLO is the NNLO corrections. The only definite way is to calculate them. In our approach, this means to calculate the real part of $K^+ \rightarrow \pi^+\pi^0\pi^0$ at two-loop in the isospin conserving limit and make the same analysis that we have done but at NNLO.

Meanwhile, we can just use the following estimate. Going from one order to the next one in our approach implies that new topologies with an extra $\pi\pi$ scattering vertex are needed. For instance, topology B in Figure 1 appears in the case of LO to NLO, and analogously in the case of NLO to NNLO. Therefore, the naive estimate of NNLO re-scattering effects coincides with the one made in [15], i.e., NNLO re-scattering effects would be suppressed by a_i^2 which respect to LO, in fact one can expect a typical 5 %

theoretical uncertainty intrinsic of any NLO approximation of the cusp effect. Again, it is possible to check this naive estimate by doing a two-loop calculation of the real part of $K \rightarrow 3\pi$ in the isospin limit and going one order further in our approach.

A further source of error in the final determination of the scattering length $a_0 - a_2$ from a fit to the cusp effect below threshold is due, as already discussed in [15], to the existence of different strategies to do the fit. The three basic ones are:

- One can consider all the a_i as free parameters in (4.12).
- All a_i are fixed to their standard values except the combination $a_0 - a_2$ in a_x that is extracted from the fit.
- One can use CHPT as much as possible. Since the combination $a_0 - a_2$, i.e. $a_x(s_3)$ only appears in \overline{B}_{00+} to which the cusp effect is proportional at this order, it is enough to keep this function \overline{B}_{00+} in terms of the scattering lengths. So that, for $\text{Im} \overline{A}_{00+}$, we can use the CHPT predictions at NLO in [5, 9].

The comparison of the results for a_x obtained from these different fit strategies will provide us with another handle to estimate the accuracy of the method. This uncertainty will become clear once the fits that we propose are done with data and to be added to the previous ones.

We want now to summarize the uncertainties that we have discussed and give our estimate for the total theoretical uncertainty. First, the final error from the fitting to $\text{Re} \overline{A}_{00+}$ including the accuracy of the formula used to do the fit, the accuracy of the data should be at the level of a few per cent. This has to be checked once the real fit is done but we believe that it is realistic to assume that this theoretical uncertainty is around 2 %.

If this is added to the 5 % of canonical uncertainty assigned to NNLO we get a theoretical uncertainty for the scattering lengths from the cusp effect in $K^+ \rightarrow \pi^+ \pi^0 \pi^0$ between somewhat larger than 5 % (if uncertainties are added quadratically) and 7 % (if linearly), i.e., we essentially agree therefore with the uncertainty quoted by [15]. However, we get our final theoretical uncertainty as the sum of several ones of order 1% to 2% to the canonical NNLO 5 % uncertainty, then a conservative attitude would be to take the linearly added uncertainty as the final theoretical one.

Yet, as noted above, we find numerical differences between our approach and the one in [15] of the same order as the NNLO quoted error. These numerical differences are just due to the different analytic form used for $\text{Re} \overline{A}_{00+}$ –either a quadratic polynomial for s_3 in [15] or the NLO in CHPT result here. In both cases all parameters are fitted to data.

To the uncertainties discussed above, one still has to add the one from the different data fitting strategies described in this section.

In this analysis of the theoretical uncertainties, we do not include the analytical discrepancy we found for $\text{Re} \overline{B}_{00+}$ above threshold as explained. This is an important issue which can only be clarified with a full NNLO calculation of the real part.

4.2 Cabibbo's Proposal for Neutral Kaons

In the neutral kaon channel it is also possible to measure the scattering lengths combination $a_0 - a_2$ from the cusp effect in the energy spectrum of two π^0 of $K_L \rightarrow \pi^0\pi^0\pi^0$. In this case the Bose symmetry of the three neutral pions implies that the amplitude is completely symmetric for the interchanges $s_1 \leftrightarrow s_2 \leftrightarrow s_3$. The amplitude can be written as

$$A_{000} = \begin{cases} \sum_{i=1,2,3} \{ \bar{A}_{000}(s_i) + v_{\pm}(s_i) \bar{B}_{000}(s_i) \} , & s_i > 4m_{\pi^+}^2 ; \\ \sum_{i=1,2,3} \{ \bar{A}_{000}(s_i) \} + iv_{\pm}(s_k) \bar{B}_{000}(s_k) + \\ + \sum_{\substack{i=1,2,3 \\ i \neq k}} \{ v_{\pm}(s_i) \bar{B}_{000}(s_i) \} , & s_k < 4m_{\pi^+}^2, \\ & k = 1, 2, 3 . \end{cases} \quad (4.16)$$

The crucial observation in (4.16) is that if the value of say s_k is below threshold, the other two variables s_i ($i \neq k$) are of order $(m_K^2 - m_{\pi}^2)/2$, so safely above threshold. Thus it is kinematically impossible to cross the threshold with all three variables s_i at the same time.

Let us suppose now that we look at the region where the variable s_3 is around threshold. In this region one can define,

$$\begin{aligned} \bar{A}'_{000} &= \sum_{i=1,2,3} \bar{A}_{000}(s_i) + \sum_{i=1,2} v_{\pm}(s_i) \bar{B}_{000}(s_i) , \\ \bar{B}'_{000} &= \bar{B}_{000}(s_3) . \end{aligned} \quad (4.17)$$

Equations (4.7)-(4.9) are now valid also for the decay of $K_L \rightarrow \pi^0\pi^0\pi^0$ once the substitutions $A_{00+} \rightarrow A_{000}$, $\bar{A}_{00+} \rightarrow \bar{A}'_{000}$ and $\bar{B}_{00+} \rightarrow \bar{B}'_{000}$ are done.

Again, we can write these amplitudes substituting the approximation (4.3) for the amplitudes near threshold. The amplitudes contain $\pi\pi$ re-scattering in all channels and to treat them we use full CHPT expressions when they are very far from threshold, which as explained in Section 4 is a better approximation than using scattering lengths.

Using one-loop for the real part of $K_L \rightarrow \pi^0\pi^0\pi^0$, one then finds

$$\begin{aligned} \text{Re} \bar{A}'_{000}|_{LO} &= C' (\text{Re} G_8 - G_{27}) m_K^2 , \\ \text{Im} \bar{A}'_{000}|_{LO} &= C' \left[v_{00}(s_3) a_{00}(s_3) + \frac{m_{\pi}^2}{32\pi f_{\pi}^2} (v_{00}(s_1) + v_{00}(s_2)) \right] m_K^2 (\text{Re} G_8 - G_{27}) + \\ &\quad + \frac{s_1 - m_{\pi}^2}{16\pi f_{\pi}^2} f_{000}(s_1) + \frac{s_2 - m_{\pi}^2}{16\pi f_{\pi}^2} f_{000}(s_2) , \\ \text{Re} \bar{B}'_{000}|_{LO} &= 0 , \\ \text{Im} \bar{B}'_{000}|_{LO} &= 2a_x(s_3) f_{000}(s_3) , \\ f_{000}(s) &= C' \left[\text{Re} G_8 (s - m_{\pi}^2) + \frac{G_{27}}{6(m_K^2 - m_{\pi}^2)} (s(9m_K^2 - 24m_{\pi}^2) - 5m_K^4 + \right. \\ &\quad \left. + 24m_{\pi}^2 + m_{\pi}^2 m_K^2) \right] . \end{aligned} \quad (4.18)$$

The meaning of LO here is the same that in (4.11).

The effect of the charged pion re-scattering appears also at NLO,

$$\begin{aligned}
\text{Re}\overline{A}'_{000}|_{NLO} &= \text{Re}\overline{A}'_{000}|_{LO} + [M_0(s_3) + M_0(s_1) + M_0(s_2)]|_{\mathcal{O}(p^4)}, \\
\text{Im}\overline{A}'_{000}|_{NLO} &= \text{Im}\overline{A}'_{000}|_{LO} + v_{00}(s_3)a_{00} \left[M_0(s_3) + \widetilde{M}_0(s_3) \right] |_{\mathcal{O}(p^4)} + \left[\text{Im}A_W^{(6,1)}(s_1) + \right. \\
&\quad \left. + \text{Im}A_W^{(6,2)}(s_1) + \text{Im}A_\pi^{(6,1)}(s_1) + \text{Im}A_\pi^{(6,2)}(s_1) + s_1 \rightarrow s_2 \right], \\
\text{Re}\overline{B}'_{000}|_{NLO} &= -v_{00}(s_3) \left[a_{00}(s_3)\text{Im}\overline{B}_{000}(s_3) + 2a_x(s_3)^2\text{Re}\overline{A}_{000}(s_3) \right], \\
\text{Im}\overline{B}'_{000}|_{NLO} &= \text{Im}\overline{B}'_{000}|_{LO} + 2a_x(s_3) \left[M_1(s_3) + \widetilde{M}_2(s_3) + \widetilde{M}_3(s_3)(m_K^2 + 3m_\pi^2 - 2s_3) - \right. \\
&\quad \left. - \widetilde{M}_3^s(s_3) \right] |_{\mathcal{O}(p^4)}, \tag{4.19}
\end{aligned}$$

where we neglected the contributions of three-pion cut graphs which have been shown to be very small in Appendix C. The functions $\text{Im}A_j^{(6,i)}(s)$ are given in Appendix B.2. The meaning of *NLO* here is the same that in (4.12).

In Figure 4 we show the ratio $100 \times \frac{d|\Gamma_{\text{cusp}}(s_3)|}{ds_3}$ over $\frac{d\Gamma(s_3)}{ds_3}$ using the results in (4.19) for $K_L \rightarrow \pi^0\pi^0\pi^0$. Here, Γ_{cusp} is the contribution of $v_\pm(s_3)\Delta_{\text{cusp}}(s_1, s_3)$ in (4.9) to the total $K_L \rightarrow \pi^0\pi^0\pi^0$ decay rate Γ . Above threshold the effect is extremely small and can hardly be distinguished.

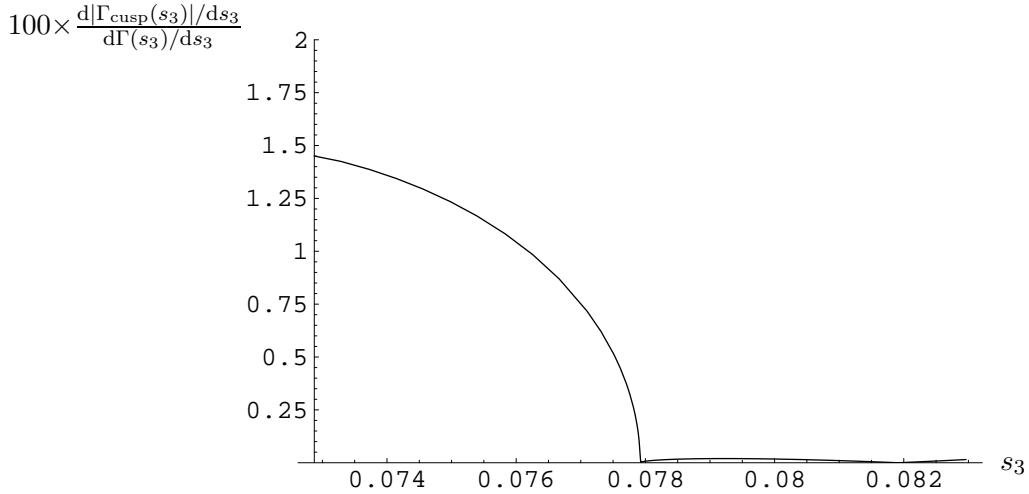


Figure 4: Plot of $100 \times \frac{d|\Gamma_{\text{cusp}}(s_3)|}{ds_3}$ over $\frac{d\Gamma(s_3)}{ds_3}$ around threshold as a function of s_3 , $4m_{\pi^0}^2 < s_3 < 4(2m_{\pi^+}^2 - m_{\pi^0}^2)$, for the decay $K_L \rightarrow \pi^0\pi^0\pi^0$.

Concerning the results of [15], we want to point out that we do not find the contributions to $\text{Re}\overline{B}_{000}$ above threshold in Equation (4.65) in that reference. We have used unphysical pion masses in order to go below threshold and still we find that unitarity cannot provide it for an analogous reason to the charged case, namely, they come from a cut where $\pi^+\pi^- \rightarrow \pi^0\pi^0$ should be below threshold and that is not physical for any values of pion masses. They again appear to come from an application of Cutkosky rules beyond unitarity and analyticity which can only be checked with a full two-loop calculation of $K_L \rightarrow \pi^0\pi^0\pi^0$.

In Figure 5 we plot the cusp effect $\frac{3N}{|C'|^2} \frac{d\Gamma_{\text{cusp}}/ds_3}{v_{\pm}(s_3)}$ in (4.9) for $K_L \rightarrow \pi^0\pi^0\pi^0$ at NLO. For numerical comparison we use the same inputs as for the charged case explained in the previous section.

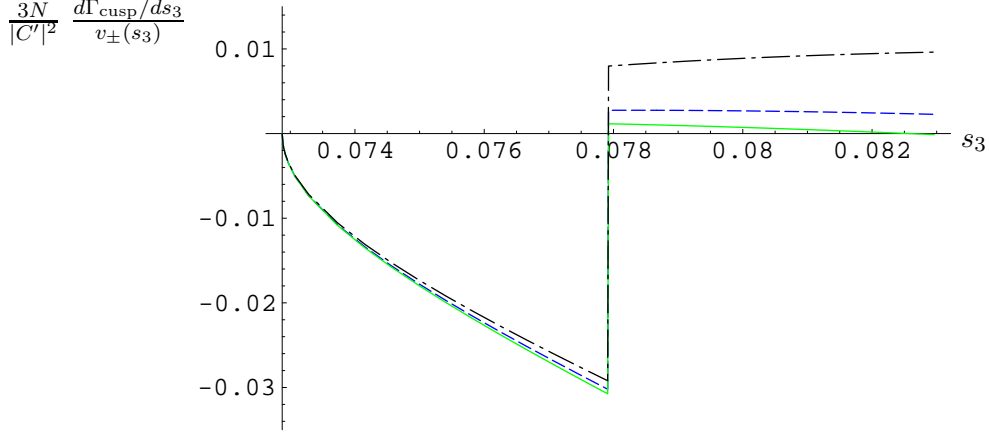


Figure 5: Plot of $\frac{3N}{|C'|^2} \frac{d\Gamma_{\text{cusp}}/ds_3}{v_{\pm}(s_3)}$ around threshold as a function of s_3 , $4m_{\pi^0}^2 < s_3 < 4(2m_{\pi^+}^2 - m_{\pi^0}^2)$ for the decay $K_L \rightarrow \pi^0\pi^0\pi^0$. The meaning of the various lines is explained in the text.

We plot $\frac{3N}{|C'|^2} \frac{d\Gamma_{\text{cusp}}/ds_3}{v_{\pm}(s_3)}$ as obtained using the results in [15] in the same two cases already explained for $K^+ \rightarrow \pi^+\pi^0\pi^0$ in Figure 3. For the slopes needed in $\text{Re}A_{000}$ in (4.6) in [15] we use the Taylor expansion of our results for $|\text{Re}A_{000}|^2 + |\text{Im}A_{000}|^2$. We have also plotted the results in [15] but without the contributions to $\text{Re}\overline{B}'_{000}$ above threshold and $\text{Re}\overline{A}'_{000}$ we do not find as explained above –this is the dashed curve. In this case, for the sake of a clearer comparison with the solid curve, we use the Taylor expansion of our results for $\text{Re}A_{000}$ to get the slopes needed in (4.6) in [15]. The difference between using either these slopes or the ones from Taylor expanding $|\text{Re}A_{000}|^2 + |\text{Im}A_{000}|^2$ are of the order or smaller than 2.5%.

If one compares now the dashed curve with the solid one, one gets differences around 1 % below threshold. The piece $\text{Im}\overline{A}'_{000} \text{Re}\overline{B}'_{000}$ which is nominally order a^3 contributes less than 1 % below threshold. Notice again that the differences between our approach and the one in [15] do not affect to the treatment of the $\pi\pi$ scattering part. These numerical differences are just due to the different analytic form used for $\text{Re}\overline{A}'_{000}$.

Above threshold, there are large numerical cancellations between $\text{Im}\overline{A}'_{000} \text{Im}\overline{B}'_{000}$ and $\text{Re}\overline{A}'_{000} \text{Re}\overline{B}'_{000}$ in (4.9). As a consequence, to predict the cusp effect above threshold for $K_L \rightarrow \pi^0\pi^0\pi^0$ with a uncertainty around 5 % one should know both the real and imaginary parts of \overline{A}'_{000} and \overline{B}'_{000} better than the 1 % level much lower than the NNLO canonical uncertainty

The effect of the pieces that we do not find in $\text{Re}\overline{B}'_{000}$ above threshold can be seen comparing the dot-dashed and the dashed curves. Below threshold the differences are not as large as for the charged case –see Figure 3. Above threshold, Δ_{cusp} is very sensitive to $\text{Re}\overline{B}'_{000}$ and the differences due to the contributions to $\text{Re}\overline{B}'_{000}$ that we do not find are much larger, see Figure 5 above threshold. However, as explained before, the data

above threshold also suffers from large theoretical uncertainties which make this region not suitable to extract the scattering lengths. The existence of these pieces is an issue which again can only be clarified with a full NNLO calculation of the real part.

Summarizing, below threshold we find comparable theoretical uncertainties for $K^+ \rightarrow \pi^+\pi^0\pi^0$ and for $K_L \rightarrow \pi^0\pi^0\pi^0$ while above threshold we found large numerical cancellations.

As for the charged case, to this uncertainty one also has to add the final error from the fitting to $\text{Re}\bar{A}_{000}$ including the accuracy of the formula used to do the fit, the accuracy of the data should be at the level of a few per cent. As said above, this has to be checked once the real fit is done but we believe that it is realistic to assume that this theoretical uncertainty is around 2 %.

If this is added to the 5 % of canonical uncertainty assigned to NNLO we get a theoretical uncertainty for the scattering lengths combination $a_0 - a_2$ from the cusp effect in $K_L \rightarrow \pi^0\pi^0\pi^0$ between somewhat larger than 5 % (if uncertainties are added quadratically) and 7 % (if linearly). I.e., we predict a similar theoretical accuracy in the extraction of $a_0 - a_2$ from neutral and charged kaon cusp effects. But notice that in the neutral case, this uncertainty just applies to the analysis of the data below threshold. As said before, there are very large numerical cancellations above threshold which preclude the use of these data.

We find numerical differences which are around 1 % between our approach and the one in [15] due to the analytic form used for $\text{Re}\bar{A}_{000}$ –either a quadratic polynomial for s_3 in [15] or the NLO in CHPT formulas. In both cases all parameters are fitted to data.

To the uncertainties discussed above, one still has to add the one from the different data fitting strategies as in Section 4.1.

5. Summary and Conclusions

In Section 3, we have presented the full FSI phases for $K \rightarrow 3\pi$ at NLO in CHPT, i.e. at $\mathcal{O}(p^6)$ analytically. The two-pion cut contributions for $K^+ \rightarrow 3\pi$ were already presented in [5]. We complete the calculation here with the three-pion cut contributions and the full result for $K_{L,S} \rightarrow 3\pi$. The two-pion cut contributions are given analytically while the three-pion cut ones are done numerically and checked always to be negligible. We used the techniques already explained in [5] which are based on perturbative unitarity and analyticity of CHPT.

In Section 4.1, we use these results to study Cabibbo’s proposal to measure the scattering lengths combination $a_0 - a_2$ from the cusp effect in the total $\pi^0\pi^0$ pair energy spectrum in $K^+ \rightarrow \pi^+\pi^0\pi^0$ [14, 15]. We studied also the analogous proposal for $K_L \rightarrow \pi^0\pi^0\pi^0$ in Section 4.2. Using the result found in Section 3 that the three-pion cut contributions are negligible –see also [15], we just include the two-pion cut contributions in the description of the cusp effect.

The cusp effect originates in the different contributions of $\pi\pi$ scattering to the $K^+ \rightarrow \pi^+\pi^0\pi^0$ and $K_L \rightarrow \pi^0\pi^0\pi^0$ amplitudes above and below threshold of $\pi^+\pi^-$ production. We obtain these contributions using just analyticity and unitarity, i.e. applying the optical

theorem above or below threshold. The optical theorem allows us to separate the real part of $K^+ \rightarrow \pi^+\pi^0\pi^0$ and $K_L \rightarrow \pi^0\pi^0\pi^0$ contributions from the $\pi\pi$ scattering which we want to measure.

We treat $\pi\pi$ scattering lengths non-perturbatively as it was done in [15] but for the real part of $K^+ \rightarrow \pi^+\pi^0\pi^0$ and $K_L \rightarrow \pi^0\pi^0\pi^0$ we use the CHPT formulas at NLO. Notice that we do not use CHPT to predict the real part of $K^+ \rightarrow \pi^+\pi^0\pi^0$ and $K_L \rightarrow \pi^0\pi^0\pi^0$, but use their analytical form at NLO to fit it to data above threshold. In [15], the authors used a quadratic polynomial to make this fit to data. We choose to use the CHPT formulas at NLO which contain the correct analytical structure at that order and can be improved by going to the next order. We studied how much differ numerically these two different choices. The treatment of $\pi\pi$ scattering is independent of these choices and we done it in the same way as in [15].

We have presented the results for $K^+ \rightarrow \pi^+\pi^0\pi^0$ in Section 4.1 and for $K_L \rightarrow \pi^0\pi^0\pi^0$ in Section 4.2. We also discussed in these sections the theoretical uncertainties for $a_0 - a_2$ if one uses our formulas to fit the experimental cusp data.

We conclude that for $K^+ \rightarrow \pi^+\pi^0\pi^0$, this uncertainty is somewhat larger than 5 % if uncertainties are added quadratically and 7 % if added linearly, always in the isospin limit. I.e., we essentially agree with the estimate in [15]. However, we get our final theoretical uncertainty as the sum of several order 1% to 2% uncertainties to the canonical NNLO 5 % uncertainty, then a conservative attitude would be to take the linearly added uncertainty as the final theoretical one.

For the case $K_L \rightarrow \pi^0\pi^0\pi^0$, we get that the uncertainty in the determination of $a_0 - a_2$ is of the same order as for $K^+ \rightarrow \pi^+\pi^0\pi^0$ if one uses the data below threshold and again in the isospin limit. Above threshold we found large numerical cancellations which preclude from using it to measure the scattering lengths combination $a_0 - a_2$.

Notice that, in addition to these uncertainties, there are numerical differences induced by using either a second order polynomial [15] or CHPT formulas at NLO, in both cases fitted to data, to describe the real part of $K^+ \rightarrow \pi^+\pi^0\pi^0$. These numerical differences are of the same order as the canonical NNLO 5 % error. The analogous differences for $K_L \rightarrow \pi^0\pi^0\pi^0$ are very small. A reason in favor of using the CHPT form at NLO is that it includes the correct analytical structure up to NLO and one can improve this systematically by going to higher orders in CHPT.

We find analytical differences for $\text{Re}\overline{B}_{00+}$ and $\text{Re}\overline{B}_{000}$ above threshold. Namely, we do not find the contributions to $\text{Re}\overline{B}_{+00}$ in (4.28) in [15] and to $\text{Re}\overline{B}_{000}$ in (4.65) in the same reference. We have just used unitarity and analyticity as explained in Section 4.1 and Section 4.2, respectively. In both cases, in order to get the contributions (4.28) and (4.65) of [15], one has to go below thresholds which are unphysical regions for any value of the pion masses. Thus, the appearance of these contributions goes beyond unitarity and analyticity and can only be checked with a full two-loop calculation of $K^+ \rightarrow \pi^+\pi^0\pi^0$ and $K_L \rightarrow \pi^0\pi^0\pi^0$.

An expansion in the scattering lengths a_i was used in [15] to obtain their NLO description of the cusp effect in $K^+ \rightarrow \pi^+\pi^0\pi^0$ and uncertainty estimate and used Feynman diagrams to do the power counting. Notice that at each higher CHPT loop order there

appear new topologies in $K \rightarrow 3\pi$ which are of order $a_i^{(n+1)}$ at the n -loop order. As a result one cannot expect to decrease the 5% theoretical uncertainty of the NLO result unless one computes the full NNLO isospin conserving $K \rightarrow 3\pi$ amplitude. We conclude that if one wants to reach the percent level in the uncertainty of the determination of $a_0 - a_2$ from the cusp effect, one would need to go to NNLO (two-loop in the dispersive part) in the re-scattering effects in the isospin limit. Recall also that a perturbative loop expansion like CHPT is not an expansion in powers of a_i .

Our CHPT approach can be improved order by order and a quantitative analysis at NNLO analogous to the one done here can provide a detailed estimate of the error at that level. Isospin breaking will at that moment be dominant and the already calculated NLO $K \rightarrow 3\pi$ isospin breaking corrections [12, 13] and other isospin breaking effects in $\pi\pi$ at threshold [20] will have to be implemented and their uncertainties added.

Finally, we believe that it is interesting to continue investigating the proposal in [14, 15] to measure the non-perturbative $\pi\pi$ scattering lengths from the cusp effect in $K^+ \rightarrow \pi^+\pi^0\pi^0$ and $K_L \rightarrow \pi^0\pi^0\pi^0$. In particular, to reduce further the theoretical uncertainties found here, a two-loop calculation in the isospin limit of those $K \rightarrow 3\pi$ is needed. Another interesting direction is to develop an effective field theory in the scattering lengths which could both check the results in [15] and allow to go to NNLO [20].

Acknowledgments

It is a pleasure to acknowledge useful discussions with Hans Bijmans, Gino Isidori and Toni Pich and informative correspondence from Jürg Gasser. This work has been supported in part by European Commission (EC) RTN Network EURIDICE Contract No. HPRN-CT2002-00311 (J.P. and I.S.), the HadronPhysics I3 Project (EC) Contract No. RII3-CT-2004-506078 (E.G.), by MEC (Spain) and FEDER (EC) Grant Nos. FPA2003-09298-C02-01 (J.P.) and FPA2004-00996 (I.S.), and by Junta de Andalucía Grant No. FQM-101 (J.P.). E.G. is indebted to the EC for the Marie Curie Fellowship No. MEIF-CT-2003-501309. I.S. wants to thank the Departament d'ECM, Facultat de Física, Universitat de Barcelona (Spain) for kind hospitality.

Appendices

A. Numerical Inputs

Here we discuss the numerical inputs we use in the numerical applications. In [9], a fit to all available $K \rightarrow \pi\pi$ amplitudes at NLO in CHPT and $K \rightarrow 3\pi$ amplitudes and slopes in $K \rightarrow 3\pi$ amplitudes was done. All these was done in the isospin limit. More recently, this fit was updated in [13] with new data on slopes and including also the full isospin breaking effects. Though our calculation of FSI at NLO uses isospin limit results we will use the results obtained in this last fit. The reason is that the change in the fit results is due to both the new data used and the isospin breaking corrections at the same level and therefore cannot be disentangled. In addition, the main isospin breaking effects due to the kinematical factors is also taken into account in our results.

	$\text{Re}\tilde{K}_i(M_\rho)$ from [13]
$\tilde{K}_2(M_\rho)$	$G_8 \times (48.5 \pm 2.4) \cdot 10^{-3}$
$\tilde{K}_3(M_\rho)$	$G_8 \times (2.6 \pm 1.2) \cdot 10^{-3}$
$\tilde{K}_5(M_\rho)$	$-G_{27} \times (41.2 \pm 16.9) \cdot 10^{-3}$
$\tilde{K}_6(M_\rho)$	$-G_{27} \times (102 \pm 105) \cdot 10^{-3}$
$\tilde{K}_7(M_\rho)$	$G_{27} \times (78.6 \pm 33) \cdot 10^{-3}$

Table 1: Results for the order p^4 counterterms $\text{Re}\tilde{K}_i$ from the fit to data done in [13]. The values of $\text{Re}\tilde{K}_i$ which do not appear are zero. For definitions of the counterterms, see [5].

and in particular the combinations in Table 1 of [5] which from the new fit in [13] are given in Table 1. These were obtained from a fit of the NLO in CHPT results to experimental data.

B. FSI at NLO for Neutral Kaon Decays: Two-Pion Cuts

Here we include the analytical results for the two-pion cuts contributions to the dispersive part of the neutral decay amplitudes at NLO in CHPT, i.e. $\mathcal{O}(p^6)$, coming from diagrams in Figure 6-7. Analogous results for the charged decay amplitudes as well as a more detailed description of the method, based on the use of the optical theorem, can be found in Appendix E of the first reference in [5]. The fully NLO FSI are completed by the calculation of the three-pion cut contributions, whose analytical results are given in Appendix C. In Subsections B.2, B.3 and B.4 we give the dispersive part of the amplitudes A_i for $K_{L,S} \rightarrow 3\pi$ denoted by $\text{Im} A_i^6$ where used the super-index 6 to indicate the CHPT order.

B.1 Notation

We use the functions M_i for the weak amplitudes already given in [9]. While We define

$$\begin{aligned} \widetilde{M}_i(s) &= \int_{-1}^1 d\cos\theta M_i(a(s) + b(s)\cos\theta)|_{p^4}, \\ \widetilde{M}_i^s(s) &= \int_{-1}^1 d\cos\theta (a(s) + b(s)\cos\theta)M_i(a(s) + b(s)\cos\theta)|_{p^4}, \\ \widetilde{M}_i^{ss}(s) &= \int_{-1}^1 d\cos\theta (a(s) + b(s)\cos\theta)^2 M_i(a(s) + b(s)\cos\theta)|_{p^4} \end{aligned} \quad (\text{B.1})$$

$$a(s) = \frac{1}{2}(m_K^2 + 3m_\pi^2 - s),$$

$$b(s) = \frac{1}{2}\sqrt{(s - 4m_\pi^2) \left(s - 2(m_K^2 + m_\pi^2) + \frac{(m_K^2 - m_\pi^2)^2}{s} \right)}. \quad (\text{B.2})$$

The amplitudes at $\mathcal{O}(p^4)$ for the $\pi\pi \rightarrow \pi\pi$ scattering in a theory with 3 flavors can be found in [8]. We decompose the amplitudes in the various cases as follows. For the case

At lowest CHPT order p^2 , the results in [13] are equivalent [using $F_0 = 87.7$ MeV] to

$$\begin{aligned} \text{Re} G_8 &= 6.6 \pm 1.1 \quad \text{and} \\ G_{27} &= 0.44 \pm 0.09. \end{aligned} \quad (\text{A.1})$$

In this normalization, $\text{Re} G_8 = 1 = G_{27}$ at large N_c . (N_c is the number of colors of QCD).

For the NLO prediction of the FSI, we only need the real part of the counterterms

$\pi^+\pi^+ \rightarrow \pi^+\pi^+$ the amplitude at $\mathcal{O}(p^4)$ is

$$\Pi_1 = P_1(s) + P_2(s, t) + P_2(s, u). \quad (\text{B.3})$$

For the case $\pi^0\pi^0 \rightarrow \pi^+\pi^-$ the amplitude at $\mathcal{O}(p^4)$ is

$$\Pi_2 = P_3(s) + P_4(s, t) + P_4(s, u). \quad (\text{B.4})$$

For the case $\pi^+\pi^- \rightarrow \pi^+\pi^-$ the amplitude at $\mathcal{O}(p^4)$ is

$$\Pi_3 = P_5(s) + P_6(s, t) + P_6(s, u) + P_7(s, t) - P_7(s, u). \quad (\text{B.5})$$

Finally, the amplitude $\pi^0\pi^0 \rightarrow \pi^0\pi^0$ at $\mathcal{O}(p^4)$ is

$$\Pi_4 = P_8(s) + P_8(t) + P_8(u). \quad (\text{B.6})$$

The value for the various P_i can be deduced from ref. [8]. In the following we use

$$\begin{aligned} \tilde{P}_i^{(n,m)}(s) &= \int_{-1}^1 d\cos\theta s^n (c(s)(1-\cos\theta))^m P_i(s, c(s)(1-\cos\theta)), \\ \hat{P}_{1,i}^{(n)}(s) &= \int_{-1}^1 d\cos\theta (c(s)(1-\cos\theta))^n P_i(c(s)(1+\cos\theta), c(s)(1-\cos\theta)), \\ \hat{P}_{2,i}^{(n)}(s) &= \int_{-1}^1 d\cos\theta (c(s)(1-\cos\theta))^n P_i(c(s)(1-\cos\theta), s), \end{aligned} \quad (\text{B.7})$$

$$c(s) = -\frac{1}{2}(s - 4m_\pi^2). \quad (\text{B.8})$$

B.2 FSI for $K_L \rightarrow \pi^0\pi^0\pi^0$ at NLO

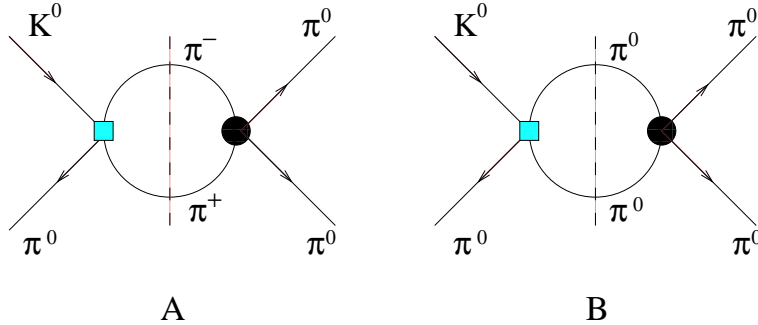


Figure 6: Diagrams for the calculation of FSI for $K_L \rightarrow \pi^0\pi^0\pi^0$ using the optical theorem. The square is the weak vertex and the circle is the strong one.

Diagrams A –two charged pions in the loop– and B –two neutral pions in the loop– in Figure 6 correspond to the two possible contributions for $K_L \rightarrow \pi^0\pi^0\pi^0$. We first compute the case when the weak vertex in Figure 6 is of $\mathcal{O}(p^4)$ and the strong vertex of $\mathcal{O}(p^2)$. The results are

$$\text{Im}A_W^{(6,1)}(s_1, s_2, s_3) = \text{Im}A_W^{(6,1)}(s_1) + \text{Im}A_W^{(6,1)}(s_2) + \text{Im}A_W^{(6,1)}(s_3),$$

$$\text{Im}A_W^{(6,1)}(s) = \frac{\sigma(s)}{16\pi f_\pi^2}(s - m_\pi^2) \left[M_1(s) + \widetilde{M}_2(s) + \widetilde{M}_3(s)(m_K^2 + 3m_\pi^2 - 2s) - \widetilde{M}_3^s(s) \right]_{\mathcal{O}(p^4)} \quad (\text{B.9})$$

$$\begin{aligned} \text{Im}A_W^{(6,2)}(s_1, s_2, s_3) &= \text{Im}A_W^{(6,2)}(s_1) + \text{Im}A_W^{(6,2)}(s_2) + \text{Im}A_W^{(6,2)}(s_3), \\ \text{Im}A_W^{(6,2)}(s) &= \frac{\sigma(s)}{32\pi f_\pi^2} m_\pi^2 \left[M_0(s) + \widetilde{M}_0(s) \right]_{\mathcal{O}(p^4)}. \end{aligned} \quad (\text{B.10})$$

Then we consider the same diagrams of Figure 6 with a weak vertex of $\mathcal{O}(p^2)$ and a strong vertex of $\mathcal{O}(p^4)$. We have

$$\begin{aligned} \text{Im}A_\pi^{(6,1)}(s_1, s_2, s_3) &= \text{Im}A_\pi^{(6,1)}(s_1) + \text{Im}A_\pi^{(6,1)}(s_2) + \text{Im}A_\pi^{(6,1)}(s_3), \\ \text{Im}A_\pi^{(6,2)}(s) &= \frac{\sigma(s)}{16\pi} (M_1(s) + M_3(s)(m_K^2 + m_\pi^2 - 3s))|_{p^2} (P_3(s) + \widetilde{P}_4^{(0,0)}(s)), \\ \text{Im}A_\pi^{(6,2)}(s_1, s_2, s_3) &= \text{Im}A_\pi^{(6,2)}(s_1) + \text{Im}A_\pi^{(6,2)}(s_2) + \text{Im}A_\pi^{(6,2)}(s_3), \\ \text{Im}A_\pi^{(6,2)}(s) &= \frac{\sigma(s)}{32\pi} (M_0(s_3) + M_0(s_1) + M_0(s_2))|_{p^2} (P_8(s) + \widetilde{P}_8^{(0,0)}(s)), \end{aligned} \quad (\text{B.11})$$

for those diagrams with two charged and two neutral pions in the loop respectively.

B.3 FSI for $K_L \rightarrow \pi^+\pi^-\pi^0$ at NLO

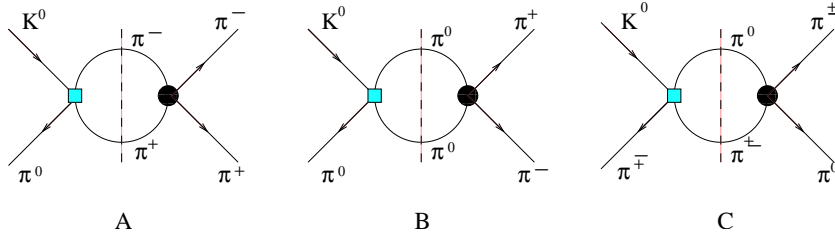


Figure 7: Diagrams for the calculation of FSI for $K_L \rightarrow \pi^+\pi^-\pi^0$ using the optical theorem. The square is the weak vertex and the circle is the strong one.

The calculation is analogous to the one for $K_L \rightarrow \pi^0\pi^0\pi^0$. The three contributions in Figure 7 correspond to two charged pions in the loop –results in Eqs. (B.12) and (B.16), two neutral pions in the loop –results in Eqs. (B.13) and (B.17)– and loops with one neutral and one charged pions. In the last case we have a S-wave contribution –results in Eqs.(B.14) and (B.18), and a P-wave contribution –results in Eqs. (B.15) and B.19), respectively. Eqs. (B.12), (B.13), (B.14), and (B.15) are the results of using the weak vertex at $\mathcal{O}(p^4)$ and the strong vertex at $\mathcal{O}(p^2)$. Eqs. (B.16), (B.17), (B.18), and (B.19) are the results of using the weak vertex at $\mathcal{O}(p^2)$ and the strong vertex at $\mathcal{O}(p^4)$.

$$\begin{aligned} \text{Im}A_W^{(6,1)} &= \frac{\sigma(s_3)}{16\pi f_\pi^2}(s_3) \left[M_1(s_3) + \widetilde{M}_2(s_3) + \widetilde{M}_3(s_3)(m_K^2 + 3m_\pi^2 - 2s_3) - \widetilde{M}_3^s(s_3) \right]_{\mathcal{O}(p^4)}, \end{aligned} \quad (\text{B.12})$$

$$\text{Im}A_W^{(6,2)} = \frac{\sigma(s_3)}{32\pi f_\pi^2} (s_3 - m_\pi^2) \left[M_0(s_3) + \widetilde{M}_0(s_3) \right]_{\mathcal{O}(p^4)}, \quad (\text{B.13})$$

$$\begin{aligned} \text{Im}A_{W,S}^{(6,3)} &= \frac{\sigma(s_1)}{32\pi f_\pi^2} (m_\pi^2 - s_1/2) \left[2M_2(s_1) + \widetilde{M}_2(s_1) + \widetilde{M}_1(s_1) \right. \\ &\quad \left. - \widetilde{M}_3(s_1)(m_K^2 + 3m_\pi^2 - 2s_1) + \widetilde{M}_3^s(s_1) \right]_{\mathcal{O}(p^4)} + s_1 \leftrightarrow s_2, \end{aligned} \quad (\text{B.14})$$

$$\begin{aligned} \text{Im}A_{W,P}^{(6,3)} &= \frac{\sigma(s_1)}{64\pi f_\pi^2} \frac{s_1(s_2 - s_3)}{s_1^2 - 2s_1(m_K^2 + m_\pi^2) + (m_K^2 - m_\pi^2)^2} \\ &\quad \times \left[(s_1 - m_K^2 - 3m_\pi^2)(\widetilde{M}_2(s_1) - \widetilde{M}_1(s_1)) \right. \\ &\quad \left. + (2s_1 - m_K^2 - 3m_\pi^2)\widetilde{M}_3(s_1) + (2\widetilde{M}_2^s(s_1) - 2\widetilde{M}_1^s(s_1)) \right. \\ &\quad \left. + (5s_1 - 3m_K^2 - 9m_\pi^2)\widetilde{M}_3^s(s_1) + 2\widetilde{M}_3^{ss}(s_1) + \frac{8}{3}b(s_1)^2 M_3(s_1) \right]_{\mathcal{O}(p^4)} \\ &\quad + s_1 \leftrightarrow s_2. \end{aligned} \quad (\text{B.15})$$

$$\text{Im}A_\pi^{(6,1)} = \frac{\sigma(s_3)}{16\pi} (M_1(s_3) + M_3(s_3)(m_K^2 + 3m_\pi^2 - 3s_3))|_{p^2} (P_5(s_3) + \widetilde{P}_6^{(0,0)}(s_3)), \quad (\text{B.16})$$

$$\text{Im}A_\pi^{(6,2)} = \frac{\sigma(s_3)}{32\pi} (M_0(s_3) + M_0(s_1) + M_0(s_2))|_{p^2} (P_3(s_3) + \widetilde{P}_4^{(0,0)}(s_3)), \quad (\text{B.17})$$

$$\begin{aligned} \text{Im}A_{\pi,S}^{(6,3)} &= \frac{\sigma(s_1)}{32\pi} \left(M_1(s_1) + \frac{1}{2}M_3(s_2)(s_1 - s_3) + \frac{1}{2}M_3(s_3)(s_1 - s_2) \right) \Big|_{p^2} \\ &\quad \times \left(\widetilde{P}_3^{(0,0)}(s_1) + \hat{P}_{1,4}^{(0)}(s_1) + \widetilde{P}_{2,4}^{(0)}(s_1) \right) + s_1 \leftrightarrow s_2 \end{aligned} \quad (\text{B.18})$$

$$\begin{aligned} \text{Im}A_{\pi,P}^{(6,3)} &= \frac{\sigma(s_1)}{64\pi} (3M_3(s_1)(s_2 - s_3))|_{p^2} \frac{1}{s_1 - 4m_\pi^2} \\ &\quad \times \left((s_1 - 4m_\pi^2)(\widetilde{P}_3^{(0,0)}(s_1) - \hat{P}_{1,4}^{(0)}(s_1) + \widetilde{P}_{2,4}^{(0)}(s_1)) + 2\widetilde{P}_3^{(1,0)}(s_1) \right. \\ &\quad \left. - 2\widetilde{P}_{1,4}^{(1)}(s_1) + 2\hat{P}_{2,4}^{(1)}(s_1) \right) + s_1 \leftrightarrow s_2. \end{aligned} \quad (\text{B.19})$$

B.4 FSI for $K_S \rightarrow \pi^+ \pi^- \pi^0$ at NLO

The diagrams contributing to this decay are the same depicted in Figure 7. The result corresponding to diagram A in Figure 7 is in Eq. B.20 for the weak vertex at $\mathcal{O}(p^4)$ and the strong vertex at $\mathcal{O}(p^2)$ and in Eq. B.23 for the weak vertex at $\mathcal{O}(p^2)$ and the strong vertex at $\mathcal{O}(p^4)$. In this case there is only P-wave contribution.

Diagram B in Figure 7 does not contribute. Diagram C in Figure 7 gives both an S-wave – results in Eqs. (B.21) and (B.24)– and a P-wave contribution – results in Eqs. (B.22) and (B.25). Equations (B.21) and (B.22) are the results of the case in which the weak vertex is at $\mathcal{O}(p^4)$ and strong vertex at $\mathcal{O}(p^2)$ in diagram C. Equations (B.24) and (B.25) are the results for the case in which the weak vertex is at $\mathcal{O}(p^2)$ and the strong vertex at $\mathcal{O}(p^4)$ in diagram C.

$$\begin{aligned} \text{Im}A_{W,P}^{(6,1)} &= \frac{\sigma(s_3)}{16\pi f_\pi^2} \frac{s_3(s_1 - s_2)}{s_3^2 - 2(m_K^2 + m_\pi^2)s_3 + (m_K^2 - m_\pi^2)^2} \left\{ a(s_3)(\widetilde{M}_4(s_3) + (2a(s_3) \right. \\ &\quad \left. - s_3)\widetilde{M}_5(s_3)) - (\widetilde{M}_4^s(s_3) + (3a(s_3) - s_3)\widetilde{M}_5^s(s_3)) + \widetilde{M}_5^{ss}(s_3) \right\} \end{aligned}$$

$$-\frac{2}{3}b(s_3)^2 M_6(s_3) \} \quad (\text{B.20})$$

$$\begin{aligned} \text{Im}A_{W,S}^{(6,2)} &= \frac{\sigma(s_1)}{64\pi f_\pi^2} (2m_\pi^2 - s_1) \left\{ 2M_4(s_1) - \widetilde{M}_4(s_1) + (m_K^2 + 3m_\pi^2 - 2s_1)(\widetilde{M}_5(s_1) \right. \\ &\quad \left. - \widetilde{M}_6(s_1)) - \widetilde{M}_5^s(s_1) + \widetilde{M}_6^s(s_1) \right\} - s_1 \leftrightarrow s_2, \end{aligned} \quad (\text{B.21})$$

$$\begin{aligned} \text{Im}A_{W,P}^{(6,2)} &= \frac{\sigma(s_1)}{32\pi f_\pi^2} \frac{s_1(s_3 - s_2)}{s_1^2 - 2s_1(m_K^2 + m_\pi^2) + (m_K^2 - m_\pi^2)} \\ &\quad \times \left\{ \frac{4}{3}b(s_1)^2 M_5(s_1) + a(s_1)(\widetilde{M}_4(s_1) - (2a(s_1) - s_1)(\widetilde{M}_5(s_1) + \widetilde{M}_6(s_1))) \right. \\ &\quad \left. - \widetilde{M}_4^s(s_1) + (3a(s_1) - s_1)(\widetilde{M}_5^s(s_1) + \widetilde{M}_6^s(s_1)) - \widetilde{M}_5^{ss}(s_1) - \widetilde{M}_6^{ss}(s_1) \right\} \\ &\quad - s_1 \leftrightarrow s_2 \end{aligned} \quad (\text{B.22})$$

$$\text{Im}A_{\pi,P}^{(6,1)} = -\frac{\sigma(s_3)}{16\pi} \frac{(M_4(s_1) - M_4(s_2))|_{p^2}}{s_3 - 4m_\pi^2} \left[(s_3 - 4m_\pi^2)\widetilde{P}_7^{(0,0)}(s_3) + 2\widetilde{P}_7^{(0,1)}(s_3) \right], \quad (\text{B.23})$$

$$\begin{aligned} \text{Im}A_{\pi,S}^{(6,2)} &= \frac{\sigma(s_1)}{64\pi} M_5(s_1)|_{p^2} (3s_1 - (m_K^2 + 3m_\pi^2))(\widetilde{P}_3^{(0,0)}(s_1) + \widetilde{P}_{2,4}^{(0)}(s_1) \\ &\quad + \widetilde{P}_{1,4}^{(0)}(s_1)) - s_1 \leftrightarrow s_2, \end{aligned} \quad (\text{B.24})$$

$$\begin{aligned} \text{Im}A_{\pi,P}^{(6,2)} &= \frac{\sigma(s_1)}{64\pi} (M_4(s_2) - M_4(s_3))|_{p^2} \frac{1}{s_1 - 4m_\pi^2} \\ &\quad \times \left((s_1 - 4m_\pi^2)(\widetilde{P}_3^{(0,0)}(s_1) - \hat{P}_{1,4}^{(0)}(s_1) + \widetilde{P}_{2,4}^{(0)}(s_1)) + 2\widetilde{P}_3^{(1,0)}(s_1) \right. \\ &\quad \left. - 2\widetilde{P}_{1,4}^{(1)}(s_1) + 2\hat{P}_{2,4}^{(1)}(s_1) \right) - s_1 \leftrightarrow s_2. \end{aligned} \quad (\text{B.25})$$

C. Three-Pion Cut Contributions to FSI

To calculate the contributions of the topologies in Figure 1 B,C and D to the FSI, we need the tree level vertices of $K \rightarrow 3\pi$ and $3\pi \rightarrow 3\pi$. The complete tree level amplitude of the $3\pi \rightarrow 3\pi$ scattering can be easily calculated using the code `Ampcalculator` developed in [21]. In this way all possible $3\pi \rightarrow 3\pi$ are included. In order to perform the integral in the phase space as prescribed in the optical theorem we assign the momentum to pions as shown in an example in Figure 8. The momentum assignment is done preserving the suffix 3 for the *odd* pion in the $K^+ \rightarrow 3\pi$ vertex.

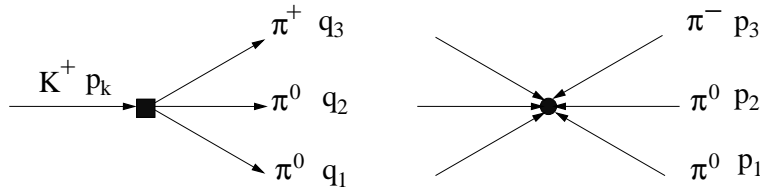


Figure 8: Example of diagram for the calculation of FSI for $K^+ \rightarrow \pi^+\pi^0\pi^0$ with momentum assignment.

In order to perform the integral in the phase space over momentum q_i it is necessary to fix a reference frame. We chose the reference frame in which the decaying kaon is at rest and the momentum p_3 defines the z-axis,

$$\begin{aligned} p_K &= (M_K, 0, 0, 0), \quad p_3 = (p_3^0, 0, 0, \bar{p}_3), \quad p_1 = (p_1^0, 0, \bar{p}_1 \sin \eta, \bar{p}_1 \cos \eta), \\ p_2 &= -p_K - p_1 - p_3 . \end{aligned} \quad (\text{C.1})$$

The momenta q_i describe also a decay of a kaon into three pions. The most general expression for these momenta, in the chosen reference frame, is

$$\begin{aligned} q_i &= R_z(\alpha)R_y(\beta)R_z(\gamma) r_i , \\ r_3 &= (r_3^0, 0, 0, \bar{r}_3), \quad r_1 = (r_1^0, 0, \bar{r}_1 \sin \theta, \bar{r}_1 \cos \theta), \quad r_2 = p_K - r_1 - r_3 , \end{aligned}$$

and $R_{z(y)}(\delta)$ are rotations around the axis z (y) of the Euler angle δ . Using the Particle Data Group (PDG) parametrization for the phase space integrals [22], the LO contribution to the $\text{Im}\bar{A}_{00+}$ and $\text{Im}\bar{B}_{00+}$ of the 3-pion cut diagrams so read

$$\begin{aligned} \text{Im}\bar{A}_{00+}^{3\pi, LO}(s_1, s_2, s_3) &= \frac{1}{16(2\pi)^5} \int dq_3^0 dq_2^0 d\alpha d\cos\beta d\gamma \left[A_{00+}^{(p^2)}(p_K, q_i) A_{3\pi,0}^{(p^2)}(q_i, p_i) \right] , \\ v_{\pm} \text{Im}\bar{B}_{00+}^{3\pi, LO}(s_1, s_2, s_3) &= \frac{1}{16(2\pi)^5} \int dq_3^0 dq_2^0 d\alpha d\cos\beta d\gamma \left[A_{++-}^{(p^2)}(p_K, q_i) A_{3\pi,\pm}^{(p^2)}(q_i, p_i) \right] , \end{aligned} \quad (\text{C.2})$$

where $A_{3\pi,0}^{(p^2)}(q_i, p_i)$, $A_{3\pi,\pm}^{(p^2)}(q_i, p_i)$ are the tree level amplitudes for $\pi^0\pi^0\pi^+ \rightarrow \pi^0\pi^0\pi^+$ and $\pi^+\pi^+\pi^- \rightarrow \pi^0\pi^0\pi^+$. At this order there are no contributions of these topologies to $\text{Re}\bar{B}_{00+}$. We have computed numerically the integrals in Eq. C.2. The correction induced by Eq. C.2 to the other LO terms is always much below the 0.5%. We find so perfectly consistent to omit these corrections at this level of precision. Similar expressions and conclusions hold for the FSI in the decay of $K_L \rightarrow \pi^0\pi^0\pi^0$. For this case one has just

$$\begin{aligned} \text{Im}\bar{A}_{000}^{3\pi, LO}(s_1, s_2, s_3) &= \frac{1}{16(2\pi)^5} \int dq_3^0 dq_2^0 d\alpha d\cos\beta d\gamma \left[A_{000}^{(p^2)}(p_K, q_i) \tilde{A}_{3\pi,0}^{(p^2)}(q_i, p_i) \right] , \\ v_{\pm} \text{Im}\bar{B}_{000}^{3\pi, LO}(s_1, s_2, s_3) &= \frac{1}{16(2\pi)^5} \int dq_3^0 dq_2^0 d\alpha d\cos\beta d\gamma \left[A_{+-0}^{(p^2)}(p_K, q_i) \tilde{A}_{3\pi,\pm}^{(p^2)}(q_i, p_i) \right] , \end{aligned} \quad (\text{C.3})$$

where $\tilde{A}_{3\pi,0}^{(p^2)}(q_i, p_i)$, $\tilde{A}_{3\pi,\pm}^{(p^2)}(q_i, p_i)$ are the tree level amplitudes for $\pi^0\pi^0\pi^0 \rightarrow \pi^0\pi^0\pi^0$ and $\pi^+\pi^-\pi^0 \rightarrow \pi^0\pi^0\pi^0$.

References

- [1] G. Ecker, hep-ph/0011026; A. Pich, hep-ph/9806303.
- [2] G. Ecker, Prog. Part. Nucl. Phys. **35** (1995) 1; E. de Rafael, hep-ph/9502254; A. Pich, Rept. Prog. Phys. **58** (1995) 563.
- [3] S. Weinberg, Physica **A 96** (1979) 327.

- [4] J. Gasser and H. Leutwyler, *Annals Phys.* **158** (1984) 142; *Nucl. Phys.* **B 250** (1985) 465.
- [5] E. Gámiz, J. Prades and I. Scimemi, *J. High Energy Phys.* **10** (2003) 042; hep-ph/0410150; hep-ph/0305164.
- [6] I. Scimemi, E. Gámiz and J. Prades, *Proc. of the 39th Rencontres de Moriond on Electroweak Interactions and Unified Theories*, p. 355, The Gioi Publishers (2005), hep-ph/0405204.
- [7] J. Prades, E. Gámiz and I. Scimemi, *Proc. of QCD'05, Montpellier*, 4-8 July 2005, hep-ph/0509346.
- [8] V. Bernard, N. Kaiser and U.-G. Meißner, *Nucl. Phys.* **B 357** (1991) 129.
- [9] J. Bijnens, P. Dhonte and F. Persson, *Nucl. Phys.* **B 648** (2003) 317.
- [10] J. Kambor, J. Missimer and D. Wyler, *Nucl. Phys.* **B 346** (1990) 17; *Phys. Lett.* **B 261** (1991) 496.
- [11] J. Kambor, J.F. Donoghue, B.R. Holstein, J. Missimer and D. Wyler, *Phys. Rev. Lett.* **68** (1992) 1818.
- [12] J. Bijnens and F. Borg, *Nucl. Phys.* **B 697** (2004) 319; *Eur. Phys. J.* **C 39** (2005) 347; A. Nehme, *Phys. Rev.* **D 70** (2004) 094025.
- [13] J. Bijnens and F. Borg, *Eur. Phys. J.* **C 40** (2005) 383.
- [14] N. Cabibbo, *Phys. Rev. Lett.* **93** (2004) 121801.
- [15] N. Cabibbo and G. Isidori, *J. High Energy Phys.* **03** (2005) 021.
- [16] G. D'Ambrosio, G. Isidori and N. Paver, *Phys. Lett.* **B 273** (1991) 497.
- [17] J.R. Batley *et al.* [NA48/2 Collaboration], *Phys. Lett.* **B 633** (2006) 173; S. Giudici [NA48/2 Collaboration], hep-ex/0505032.
- [18] G. Colangelo, J. Gasser and H. Leutwyler, *Phys. Lett.* **B 488** (2000) 261, *Nucl. Phys.* **B 603** (2001) 125.
- [19] J.R. Peláez and F.J. Ynduráin, *Phys. Rev.* **D 71** (2005) 074016; hep-ph/0412320.
- [20] G. Colangelo, J. Gasser, B. Kubis, and A. Rusetsky, in preparation.
- [21] R. Unterdorfer and G. Ecker, *J. High Energy Phys.* **10** (2005) 017.
- [22] S. Eidelman *et al.* [Particle Data Group], *Phys. Lett.* **B 592** (2004) 1.